Experimental investigation on the durability of a novel lightweight prefabricated reinforced-EPS based construction system

Experimental investigation on the durability of a novel lightweight prefabricated Reinforced-EPS based construction system

M. D'Orazio[a], P. Stipa[b], S. Sabbatini[b], G. Maracchini[a]*

[a] Department of Civil and Building Engineering and Architecture (DICEA), Polytechnic University of Marche, via Brecce Bianche, 60131, Ancona, Italy
[b] Department of Materials, Environmental Sciences and Urban Planning (SIMAU), Polytechnic University of Marche, via Brecce Bianche, 60131, Ancona, Italy

*corresponding author. *E-mail address*: g.maracchini@staff.univpm.it
E-mail addresses: m.dorazio@staff.univpm.it; p.stipa@univpm.it; s.sabbatini@univpm.it; g.maracchini@staff.univpm.it

ABSTRACT

This paper investigates the durability of a low-cost construction system named HOMEDONE developed to realize affordable and also temporary housing solutions. The system is based on the assembly of 3D-reinforced EPS panels externally topped off with a multi-layer rendering system. Similar technologies showed durability issues, especially in hot climates, due to the thermal and hygrometric stresses of the thin finishing layers when coupled to thick EPS panels and exposed to extreme events. For this reason, in this work freeze-thaw and wet/drying-UV aging tests on HOMEDONE panels with different finishing systems have been carried out, monitoring macroscopic, microscopic (ATR-FT-IR analysis) and bond strength variations due to aging. Results have pointed out good mechanical properties of the system and only small color variations of the finishing layer due to UV cycles. Then, HOMEDONE can be considered as a durable option for affordable and temporary housing solutions.

KEYWORDS

Affordable housing; Temporary housing; Reinforced EPS; Prefabricated; Durability; Pull-off; ATR-FT-IR spectroscopy; XRD analysis

1 INTRODUCTION

Durability is one of the most important criteria for materials selection in building constructions. The natural deterioration of building components, in fact, leads to a loss of performance of these elements, affecting their original characteristics and compromising the fulfillment of specific requirements during building service life.

Roofs and external walls are the building components most affected by durability issues since directly exposed to the most aggressive actions (climate, impact, etc.) [1–3]. These elements, however, have also important functions such as protection, thermal insulation and watertightness, which must be guaranteed for a specified minimum period of time [4]. Then, it is important to investigate their durability, suitability for use and aging processes, even in order to optimize the adoption of preventive and effective interventions.

With this aims, a lot of studies in literature investigated the durability of traditional roof and walls components, mainly focusing on the behavior under extreme environmental conditions of their covering materials, such as mortars, ceramic tiles, natural stone, ETICS, wood panels, curtain walls and ventilated façades (see e.g. [1–3,5–9]).

However, the increasing global need of affordable housing [10,11] and temporary accommodations for post-disaster scenarios (increasingly frequent due to climate change [12,13]) are pushing the research towards the development of new and non-traditional low-cost building components, whose durability is often treated as a secondary aspect [14,15]. In particular, about 330 million urban households around the world live today in inadequate housing or are financially overstretched by housing costs [16–18] and 106 million additional households, i.e. about 1.6 billion additional people, will face the affordability challenge in 2025 [16,19,20]. In addition, over 60 million of displaced people are living in low-cost temporary accommodations, in which forcibly displaced people may end up living for years or even decades [21–25]. In this framework, it is imperative for cities and governments to develop and provide durable and low-cost housing solutions for the lower-income and poorest population and for displaced people, in order to curb the growth and creation of slums, to ensure a resilient and sustainable urban development and to respect the everyone's right to have an adequate standard of living [16].

Lightweight prefabricated construction systems are often proposed as an affordable housing solution, to solve the increasing global housing demand, and as temporary housing units in emergency scenarios [10,11,26,27]. Thanks to the simultaneous adoption of prefabrication and value engineering, in fact, these technologies allow reducing delivery time and costs by up to 50 and 30%, respectively [16]. In particular, the use of standardized and prefabricated units or elements allows not only a quick, inexpensive and on a larger scale delivering, but also the reduction of energy consumption and wastes during the construction stages [28,29] due to the improvement of worksite safety, productivity and quality [30–32]. The impact of the buildings at the end of their life is also minimized due to the possibility of disassembling and/or

relocating the prefabricated modules [33–35]. Value engineering, instead, allows meeting specific economic targets through the minimization of not strictly necessary costs. This is usually obtained by "de-specifying" building requirements, such as, for example, minimum ceiling heights, amount of electrical or plumbing fixtures, but also varying characteristics of building components, favoring the use of cheaper ones [16].

Due to this, it is not uncommon that durability issues may occur during the service life of these buildings, especially if an adequate investigation on the aging processes of these low-cost building components is not accurately carried out [36]. Studies on affordable or temporary lightweight construction systems, in fact, often neglect durability aspects, mainly focusing on energy performance and thermal comfort (see e.g. [22,34,36–43]). An adequate investigation on durability aspects of these new building components and construction systems is then strongly needed to ensure a specific building performance and to predict correctly their actual life span, but also to avoid undesirable maintenance and repairing costs during their service life and to assess efficiently their life cycle cost and environmental impact [15,35].

This paper presents the research results of an experimental campaign aimed at investigating the durability in outdoor environments of a novel EPS-based lightweight prefabricated construction system, named HOMEDONE, specifically developed for affordable housing and temporary accommodation. The HOMEDONE construction technology is based on the assembly of prefabricated structural reinforced-EPS panels internally reinforced with a 3D steel wire mesh and externally topped off with a thin and continuous multi-layer rendering system. This system can be used to obtain in a few days even multi-story buildings, and several buildings were just built to obtain low-cost districts in developing countries and temporary emergency camps in post-earthquake scenarios [44].

As evidenced by similar technologies that adopt thin multilayer rendering systems on EPS panels (for which, however, a satisfactory body of knowledge about their long-term properties and durability is still lacking [45,46]), the durability of the HOMEDONE system is strongly related to the durability of its external finishing layers [47–52]. In fact, due to the high thermal resistance of the EPS panels, the outermost rendering layer reaches very high temperatures in summer (even 70°C), which can suddenly drop when, for example, a rainstorm occurs [37,53,54]. These high-temperature variations, along with the water content variations, cause different deformations among layers that may cause cracks or detachments of the finishing layers from the background [3,5,6,50,55]. Clearly, since the studied system is composed of a set of panels whose external continuity is ensured only by the external finishing system, these cracks may turn in (or be a symptom of) a loss of performance of the entire system [45,48,49,55–57]. Then, it is important to investigate the possible occurrence of cracks and detachments on the external rendering systems.

With this aim, in this work, the thermal compatibility among the different layers of the HOMEDONE construction system is investigated with appropriate accelerated aging tests, i.e. freeze-thaw tests and wet/drying and UV tests. These tests involve the most relevant atmospheric agents affecting the durability of EPS walls with multilayer rendering systems, such as thermal shocks, UV radiation and variations in water contents (driving rain) [3,8,9,47,58], excepting for physical and chemical agents such as pollutants that have been not considered in this study [48]. During tests, the development of cracking, detachments and variations in bonding strength between different layers have been then measured. Attenuated Total Reflection Fourier-Transform Infrared (ATR-FT-IR) spectroscopic analyses have been carried out to understand the effects of aging processes on a micro-scale [59–61]. X-Ray Diffraction (XRD) and ATR-FT-IR analyses have been also carried out to characterize the different finishing materials. This experimental campaign represents the initial stage of a wider research program on the hygrothermal performance of HOMEDONE panels [62].

2 MATERIALS AND METHODS

2.1 Phases

This paper can be subdivided into two main phases.

In the first phase, a characterization of the different finishing materials applied on the EPS-reinforced panels is carried out through X-Ray Diffraction (XRD) and Attenuated Total Reflectance Fourier Transform Infrared Spectroscopy (ATR-FT-IR) analyses in order to evaluate their composition and to extend the findings to broader applications.

In the second phase, the effects of atmospheric agents (such as thermal shock, UV radiation, driving rain, etc. [48]) on the HOMEDONE panels have been evaluated by carrying out aging tests typically adopted in literature for similar technologies [3,8,9,47,58]. In particular, considering the absence of specific standards for reinforced-EPS construction systems, testing procedures commonly adopted for assessing the thermal compatibility between rendering systems and different substrates (as EPS [63–65] and concrete [66]) have been taken as reference, i.e.:

- Freeze-Thaw tests according to EN 13687-4:2003 [66];
- Wet/Drying and UV tests according to EN ISO 16474-3:2016 [67].

The effects of the two different aging cycles on the external layers of the samples have been monitored by using both non-destructive and destructive tests. Firstly, macroscopic variations of the external layers caused by aging have been assessed by spectrophotometric analyses (in the visible wavelength range) and visual inspections. Then, changes on the microstructure, which have an important meaning for macroscopic properties such as strength, water absorption, frost-proof, etc. [6], have been assessed by using ATR-FT-IR analyses [59–61]. Finally, since bond strength is a key factor for determining the thermal compatibility between layers of a wall covering [68], bond strengths have been also determined through pull-off tests after Freeze-Thaw tests, as prescribed in EN 13687-4:2003 [66].

2.2 HOMEDONE construction system

The HOMEDONE construction system is a lightweight relocatable prefabricated construction system based on the assembly of prefabricated reinforced-EPS panels. Specifically developed for affordable and temporary housing solutions, it takes advantage of industrial automated construction processes and value engineering to reduce housing delivery time and costs. In particular, it allows delivering both ready-made units (totally made off-site and then shipped on-site) and kit supplies (involving the shipping of prefabricated and modular elements for the on-site assembly). The latter are very useful for areas where, due to difficult access, heavy transport systems such as crane cannot be used [69].

Each reinforced-EPS panel (Fig. 1b) consists of a high strength tridimensional electro-welded galvanized steel wire (S235JR [70] steel bars with a diameter of 3 mm), embedded in a high-density EPS panel (from 45 kg/m^3 to 65 kg/m^3).

Depending on the structural and architectural needs, the panels and the embedded steel wires can be provided in different shapes and dimensions, allowing the construction of buildings of any size. The steel mesh is provided with metal joints, designed to easily connect roof and wall panels. Thanks to a patented hooking system, in fact, panels can be manually assembled on-site by using a simple Allen wrench (Fig. 1). This is very useful in emergency situations or, in general, in places where skilled workers are not present as in developing countries [71].

After the assembling, the external surfaces are topped off with a continuous thin multi-layer rendering system (with an overall thickness of 4 mm [68]). This latter includes three layers: a cement-based base coat reinforced with a glass fiber mesh (generally 5x5mm); a key coat, which acts as a preparation for the application of a finishing coat; a finishing coat, which contributes to the protection against weathering and provides a decorative finish (Fig. 1b). Due to its lightweight, the assembled building can be easily relocated and different units can be combined with each other to meet the needs of the inhabitants or to allow different use (i.e. temporary housing, affordable housing or for tourism).

In order to study the durability of the system, in this work, a single panel typically adopted for one-story constructions is taken as reference. This panel is characterized by a thickness equal to 10 cm and an EPS density of 45 kg/m^3. The dimensional characteristics of the tridimensional steel wire are reported in Fig. 2.

As previously said, the weakest part of this construction system is the external multi-layer rendering system, i.e. that directly exposed to the weathering action. In the external surface, in fact, very high temperature and water content variations can occur, due to the high thermal resistance of the structural EPS panels. For this reason, different finishing systems have been considered in this study, i.e. those directly provided by the HOMEDONE manufacturer for different climatic conditions, in order to identify the most suitable for use. In particular, these systems involve three different cement-based base coat mortars and five different types of white finishing coats.

Base coats are made of a ready dry mixture of cement binder and sand fillers smaller than 0.5, 0.7 and 1.2 mm for the basecoat 1, 2 and 3, respectively. The adopted finishing coats, instead, are characterized by different resin types, i.e. acrylic (A1 and A2), acrylic siloxane (AS and S) and styrene-acrylic (StA) resins. It is known, in fact, that different resin types may behave differently when subjected to aging cycles [5,47]. The main characteristics and the nomenclatures of the multi-layer rendering systems subject to the aging test are listed in

Table 1. For the sake of brevity, the key coats are not reported since strictly related to the related finishing coat.

Before carrying out aging tests, qualitative and quantitative information on the thermal performance variation of the chosen panel, due to the presence of the embedded steel bars have been collected. In particular, first a qualitative estimation of the surface temperatures variation on the panel surface was obtained through an active infrared thermographic analysis on a panel purposely heated at 55°C [72–74]. At this aim, a *Mikron 7800 Infrared Camera* was used, while climatic data, emissivity value (set equal to 0.95 [75]) and the distance of the thermal camera from the target area were set up into the *NRG Pro software v.1.997* to obtain a good estimation of the temperatures. Then, in order to evaluate the thermal performance variation of a panel in real use conditions, surface temperatures and heat fluxes were measured in different points of a real panel used to build an experimental mock-up (see [62]). As a result, the IR camera showed a temperature difference on the panel surface of about 0.25°C when the IR photo was taken (Fig. 3). The *in situ* survey showed no significant variations between the measured surface temperatures and between heat fluxes, denoting a sufficiently good homogeneity of the panel in terms of thermal performance in real use conditions [62].

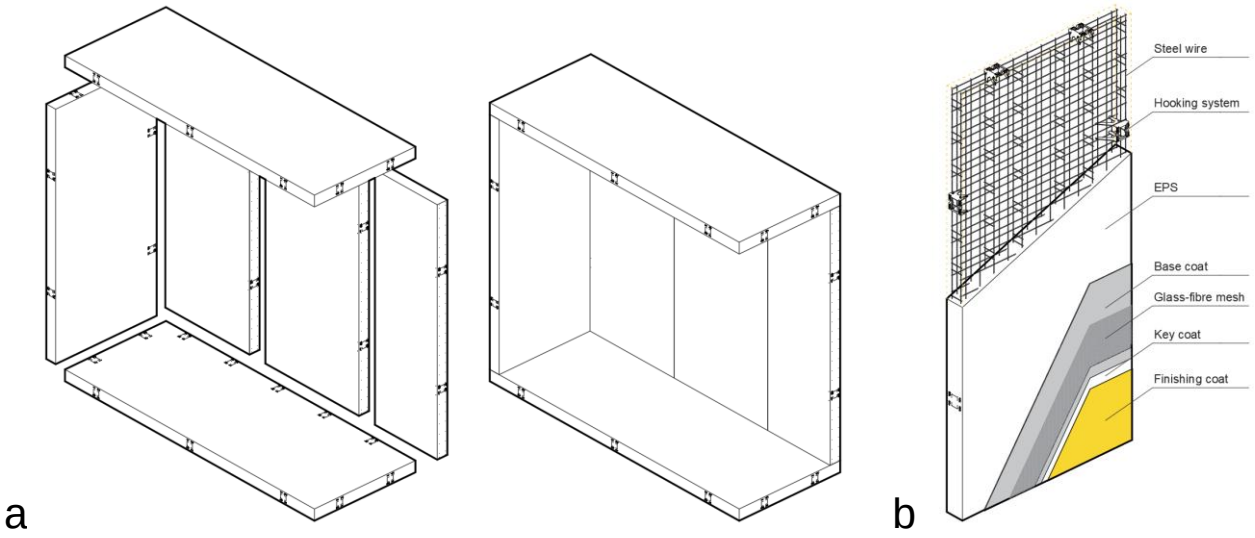

Fig. 1. a) Axonometric view of the assembly process of reinforced-EPS panels; b) axonometric view of reinforced-EPS panels adopted in this study with the description of the multi-coat rendering system.

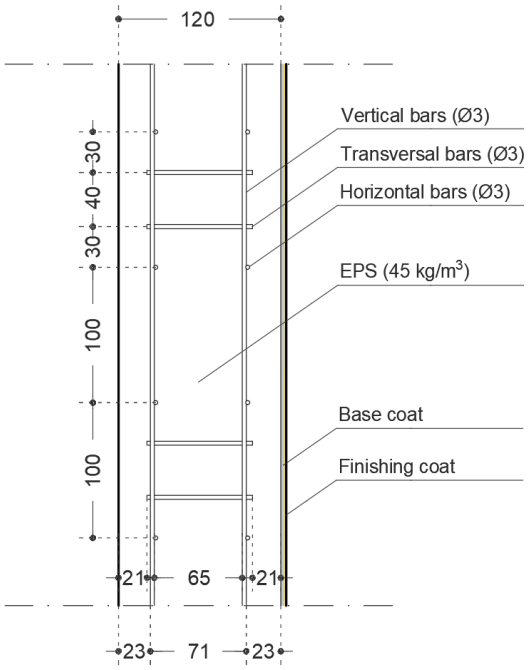

Fig. 2. Main geometrical data of the reinforced-EPS panels adopted in this study. Dimensions in millimeters.

Table 1. Identification and composition of the HOMEDONE multi-layer rendering systems with the most relevant properties according to the technical datasheets.

Rendering system ID	Base coat			Finishing coat				
	ID	Width (mm)	ETA	ID	Kind of resin	Width (mm)	ETA	Fibred
1-AS	1	3±0.2	06/0149	AS	Acrylic siloxane	1.2±0.2	08/0252	Yes
1-A1				A1	Acrylic	1.2±0.2	07/0200	Yes
1-A2				A2	Acrylic	1.5±0.2	-	No
1-StA				StA	Styrene acrylic	1.2±0.2	-	Yes
2-AS	2	3±0.2	-	AS	Acrylic siloxane	1.2±0.2	08/0252	Yes
2-A1				A1	Acrylic	1.2±0.2	07/0200	Yes
2-S				S	Acrylic siloxane	1.0±0.2	07/0200	No
2-StA				StA	Styrene acrylic	1.2±0.2	-	Yes
3-AS	3	3±0.2	04/0033	AS	Acrylic siloxane	1.2±0.2	08/0252	Yes
3-A1				A1	Acrylic	1.2±0.2	07/0200	Yes
3-S				S	Acrylic siloxane	1.0±0.2	07/0200	No
3-StA				StA	Styrene acrylic	1.2±0.2	-	Yes

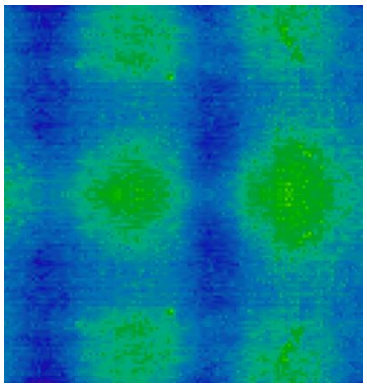

Fig. 3. Thermal IR image of the heated sample. Surface temperatures vary from about 23.75 °C (dark blue points) to about 24.00 °C (light green points).

2.3 Material characterization

2.3.1 X-ray diffraction (XRD) analyses

X-ray diffraction (XRD) is a powerful nondestructive technique for material characterization based on Bragg's law, able to provide information on structures, phases, preferred crystal orientations (texture), as well as average grain size, crystallinity, strain and crystal defects [3,5,76]. In particular, a monochromatic beam of X-rays is projected into the sample, and the reflected X-rays are then analyzed by a detector. A diffraction pattern is thus obtained, which can be considered as a fingerprint of the periodic atomic arrangements of the material under investigation, where broad peaks are produced by the amorphous regions of the samples while sharp peaks are produced by the crystalline regions.

In this study, XRD analyses have been carried out on powdered hydrated base coats samples in order to evaluate the microstructural composition of the adopted base coats materials before aging [3,5]. At this aim, an X-Ray diffractometer *RX Philips PW 1730*, with CuKa radiation, have been used, scanning at a diffraction interval of 5–70° with speed of 0.2°/min at 40kV voltage and 30 mA current intensity.

2.3.2 Attenuated Total Reflection Fourier Transform IR (ATR-FT-IR) spectroscopy

Attenuated Total Reflection Fourier Transform IR (ATR-FT-IR) spectroscopy is a sampling technique used in conjunction with infrared spectroscopy, in transmission or reflection modes, which enables samples to be examined directly in the solid or liquid state without further preparation [59].

An ATR accessory operates by measuring the changes occurring in a totally internally reflected infrared beam after interacting with the sample: the beam is directed onto an optically dense crystal with a high refractive index at a certain angle. This internal reflectance creates an evanescent wave that extends beyond the surface of the crystal into the sample in contact with it. In those regions of the IR spectrum in which the sample absorbs energy, the evanescent wave will be attenuated, returns back to the crystal, then exits in the opposite end towards the detector of the IR spectrometer which, in turn, records the attenuated beam as an interferogram, which is further transformed (FT) in an IR spectrum. For ATR measurements, the infrared beam protrudes only a few microns (0.5 μm - 5 μm) beyond the crystal surface and into the sample, hence the penetration depth of IR light is independent of the sample thickness.

In this study, ATR-FT-IR measurements have been carried out to acquire the spectra of the resins 1A2 (acrylic resin), 2A1 (acrylic resin), 2S (acrylic siloxane resin), 2StA (styrene-acrylic resin) and 2AS (acrylic siloxane resin) reported in

Table 1. Spectral analyses have been carried out both on the original resin samples, used as controls, and on those subjected to aging treatments through freeze-thaw cycles (FT) and UV-wetting cycles (UV), in order to determine the occurrence of microscopic variation after aging.

The samples have been analyzed by means of a *Perkin-Elmer Spectrum GX FT-IR System* spectrophotometer equipped with ATR single reflection diamond (*Senior Tecnologies DURA SamplIR II*) in the range between 4000 – 500 cm^{-1}, with a spectral resolution of 4 cm^{-1} and recording 32 scans. For this kind of measurement, the samples have been directly deposited on the measuring surface without requiring any preparation. In particular, a small amount of each resin has been placed on the ATR crystal and measurement has been carried out immediately. Identical experimental conditions have been maintained for all samples, and the background adsorption spectrum has been recorded each time for correction. *Spectrum 5.3.1* (*Perkin-Elmer*) has been used as the operating software.

2.4 Freeze-thaw test

For each applied rendering system (

Table 1), three 20x20x10 cm (B x H x W) samples have been prepared and cured for 7 days at the normalized temperature and relative humidity (RU) of the laboratory (21 ± 2 °C and 60 ± 10 %, respectively). One sample, marked as "*a_FT*" sample, has been stored in the laboratory and used as a reference sample. The other two, marked as "*b_FT*" and "*c_FT*",

have been subjected to 30 freeze-thaw cycles (Fig. 4) according to EN 13687-4:2003 [66] and EN 1504-3:2006 [77].

The effects of freeze-thaw cycles on the rendering systems have been assessed every 10 freeze-thaw cycles (i.e. at t_1, t_2 and t_3) in terms of surface defects (degree of blistering, cracking and flaking according to EN ISO 4628-1:2016 [78]) and chromatic alterations (according to ISO/CIE 11664-6:2014 [79]). The final assessment (t_3) has been carried out after 16h from the end of the last cycle [66].

In particular, digital images have been acquired through a 4800 x 9600 dpi resolution scanner (*HP G3010*) and a *Dino Lite Edge* digital microscope. In the latter case, nine 10x images of about 5x6.25 mm at nine fixed locations have been taken at each time interval.

Spectrophotometric analyses in the 340-740 nm wavelength range have been carried out by using a *Konika Minolta Cm.2600d* spectrophotometer. Colorimetric alterations have been assessed by following the CIELAB method according to ISO/CIE 11664-6:2014 [79]. The CIELAB method defines colors through three different coordinates of the CIELAB space measuring lightness (L^*), green to red (a^*) and blue to yellow (b^*) hue variations. For each specimen, and at each time interval, twenty-five measurements in terms of CIELab coordinates have been taken on twenty-five fixed locations in order to allow precise repeated measurements in the same points every time interval. Each measurement has been recorded as the mean of three. The color differences ΔE have been computed for each measuring point by comparing the measured coordinates before testing (t_0) with those measured at each time interval according to the procedure described in ISO/CIE 11664-6:2014 [79]. The differences in terms of lightness and chromaticity between two different colors, i.e. ΔL^*, Δa^* and Δb^*, have been also monitored.

Before and after aging, pull-off tests (EN 1542:1999 [80]) and ATR-FT-IR spectrophotometric analyses in the 2.5 – 20 µm (4000 – 500 cm^{-1}) wavelength range (described in section 2.5) have been also carried out. Pull-off tests are important for investigating the behavior of the wall covering material through its service life. In this study, a *CONTROLS Pull-Off/Bond strength digital tester 58-C0215* with accuracy equal to 1% has been used. In particular, according to the European Standard EN 1542:1999 [80], after a curing period of 7 days from the end of the test, five pull-off tests have been carried out on the fixed locations shown on both aged ("*b_FT*" and "*c_FT*") and not-aged ("*a_FT*") samples.

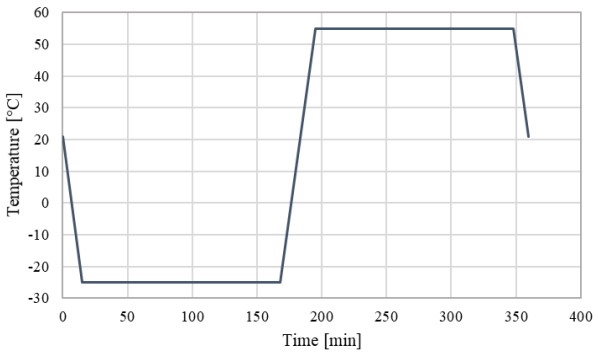

Fig. 4. Freeze-Thaw cycle adopted in this study.

2.5 Wet/drying and UV test

Wet/drying and UV tests have been carried out by taking as reference the testing procedure reported in EN ISO 16474-3:2016 [67]. In particular, for each rendering system, four 12.5x12.5x10 cm (B x H x W) samples have been prepared (Fig. 5) and cured for 7 days at the normalized temperature and RU of 23 ± 2 °C and 50 ± 5 %, respectively. According to EN 1062-11:2002 [81], three samples, marked as "*b_UV*", "*c_UV*" and "*d_UV*", have been subjected to 42 days of wet/drying and UV cycles. One sample, namely "*a_UV*", has been used as a reference sample and stored in a dark room at 23 ± 2 °C and 50 ± 5 % RU.

Each cycle of exposure has lasted 6 hours and consisted of 5 hours of UV exposure at 35 ± 3 °C and 1 hour of water spray at 25 ± 3 °C. The adopted UV lamp emits across the entire spectrum of the UV light, with peak emission in the UVA range at 366 nm. The water spray technique has been adopted for wetting the specimen due to the low conductivity of the samples [67].

The effects of thermal cycles on the external layer of the specimens have been assessed in terms of surface defects, chromatic alterations and possible changes in their FT-IR spectra. According to ISO 16474-1:2013 [82], the surfaces of the tested samples have not been washed or cleaned before the measurements. In particular, surface defects and chromatic alterations have been assessed before testing (t_0) and after every week (t_1, t_2, t_3, t_4, t_5 and t_6) by using the same instruments and methodologies described in section §0. Even in this case, the measurement points have been localized by a reference spatial grid to ensure precise repeated measurements in the same locations. Before color measurements, the specimens have been left to dry at the laboratory temperature for approximately 3h in order to minimize the color changes of the surfaces caused by the water content in the external layers. An additional color measurement has been also taken after a curing period of 24h in order to determine the color stability after exposure.

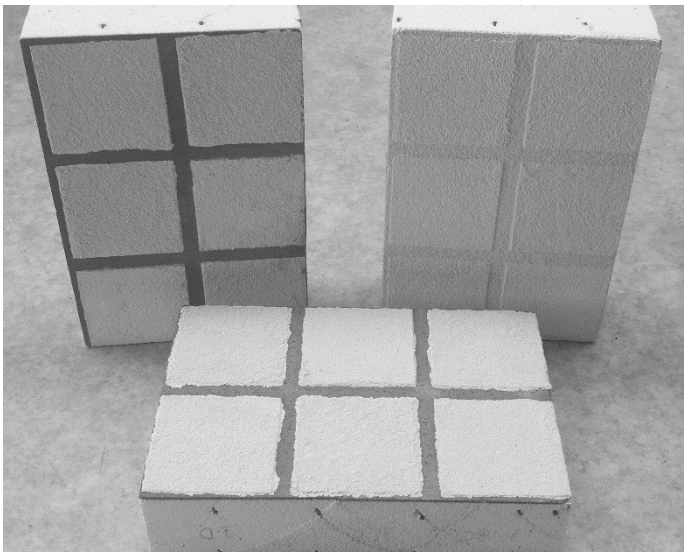

Fig. 5. Specimens prepared for the wet/drying and UV test.

3 RESULTS

3.1 Materials characterization

3.1.1 XRD analyses

Powdered samples of hydrated base coats have been investigated by means of XRD analyses spectroscopy, as described in section 2.3.1, in order to characterize the adopted base coats materials by evaluating their microstructural composition and then to extend the results to broader applications.

XRD results of the 1, 2 and 3 basecoats after 28-day of hydration are reported in Fig. 6. As expected, the diffraction bands show the presence of cement binder components like alite and calcite in all the analyzed materials, as observed for similar thin-layer plaster typically applied on EPS or cement substrates (see e.g. [5]). The basecoats mainly differ from each other due to the use of different types of sand filler. In particular, for basecoats 1 and 2, the most often detected peak is related to quartz that, along with mica, chlorite and natural silicates, indicates the use of natural silica sand filler for manufacturing the two mortars [5]. Differently, for basecoat 3, the presence of ankerite is observed, denoting the use of carbonate sand instead of silica sand [83].

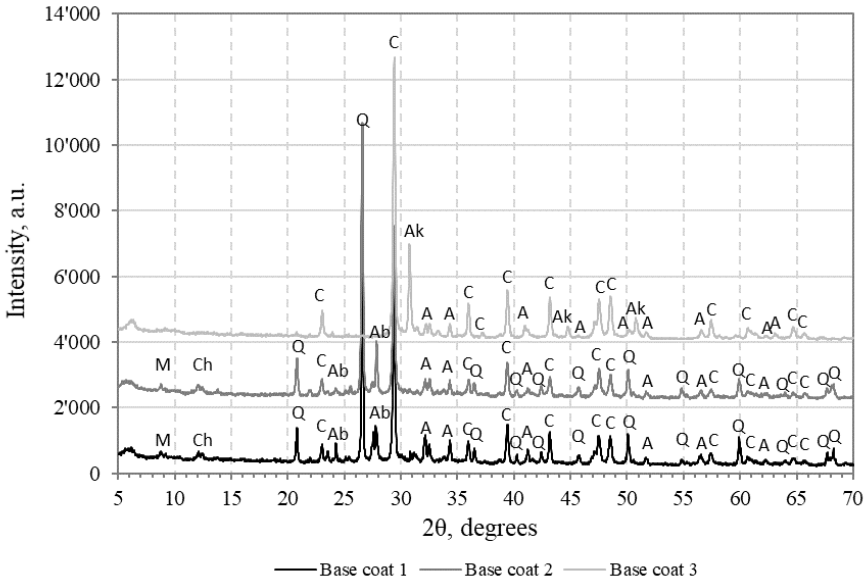

Fig. 6. XRD analysis of 1, 2 and 3 basecoats (A – Alite, C – Calcite, Q – Quartz, Ab – natural silicates (albite), M – Mica, Ch – Chlorite, Ak – Ankerite).

3.1.2 ATR-FT-IR analyses

Aliquots from the untreated samples have been investigated by means of ATR-FT-IR spectroscopy as described in section 2.3.2, in order to characterize the different samples. As a result, all resins analyzed have been found to be charged with large quantities of calcium carbonate as a filler, whose characteristic spectral bands (at 2872, 2513, 2140, 1795, 1739, 1377, 873 and 712 cm^{-1}) resulted superimposed with those corresponding to the organic matrix of each sample, hence hampering a proper characterization. In Fig. 13Fig. 7, the non-aged 2StA IR spectrum has been reported as a representative example.

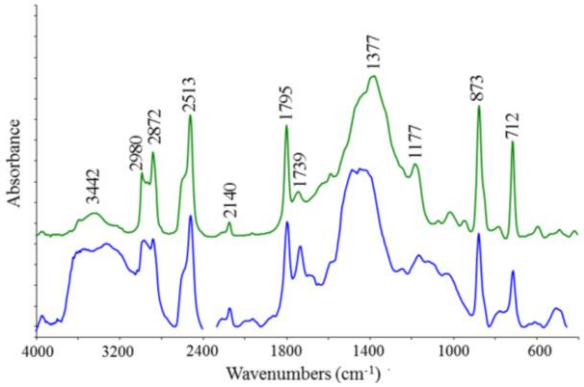

Fig. 7. IR spectra comparison of calcium carbonate alone (black), 2StA (blue), in the 4000-450 cm^{-1} region.

In order to perform a correct characterization, the organic matrix present in each sample has been separated from the calcium carbonate by overnight extraction with chloroform at room temperature. After solvent evaporation of these extracts at reduced pressure, the resulting organic residues have been analyzed in transmission mode, and the characteristic spectral bands of the polymers in the samples resulted clearly visible allowing their identification. This procedure has been successfully employed for all non-aged samples (1A2, 2A1, 2S, 2StA, 2AS), and some results have been reported in Fig. 8. In particular, the spectra of 2StA, 2S and 2A1 are shown in Fig. 8, as representative of the three different types of organic matrix found in the samples under investigation.

In particular, by comparing the spectrum of non-aged 2StA resin with those present in the database available from the instrument used (*Perkin-Elmer*), the correspondence with the spectrum of a styrene-acrylic resin was clearly evident, according to what reported in

Table 1; similarly, the spectra of 2S and 2A1 resulted attributable to an acrylic siloxane and an acrylic resin respectively.

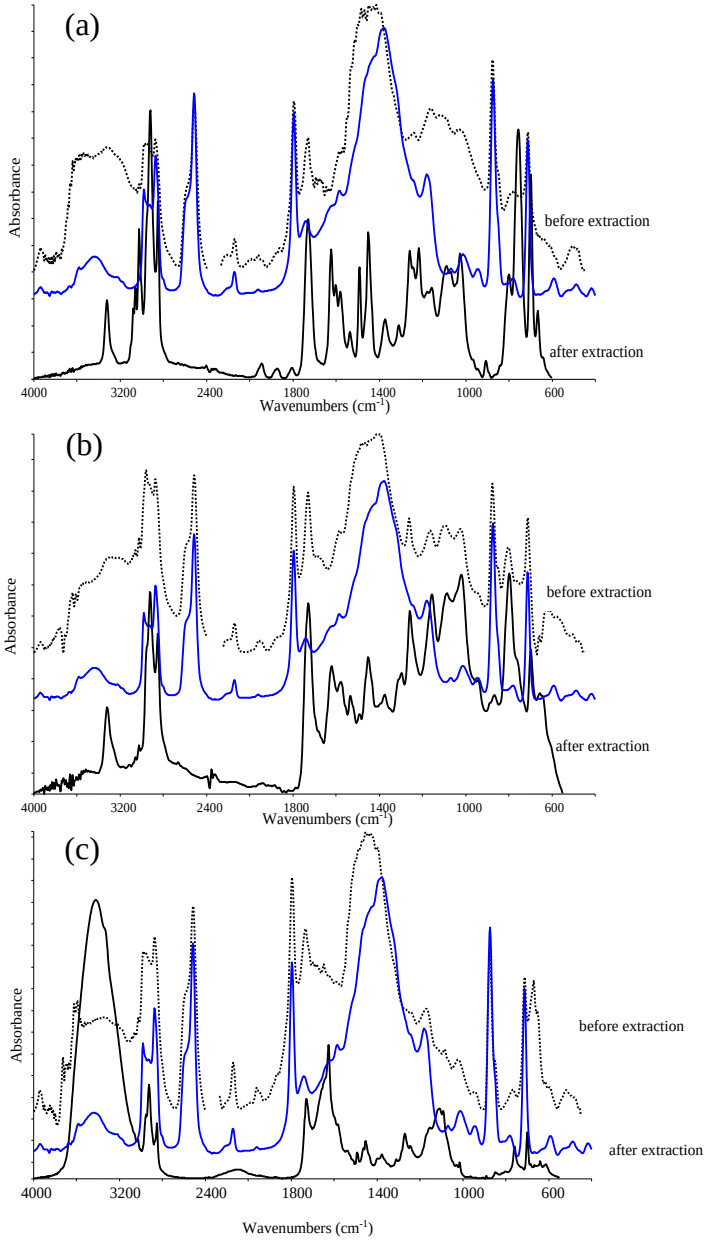

Fig. 8. Comparison between IR spectra of 2StA (a) 2S (b) and 2A1 (c) before (dotted black lines) and after (solid black lines) the extraction procedure in the 4000-450 cm^{-1} spectral region. The blue lines refer to the spectrum of pure calcium carbonate.

3.2 Freeze-thaw test

The results of visual inspections are summarized in Fig. 9, in which some representative digital image acquisitions are reported. As can be seen, the freeze-thaw cycles have not caused detachments or other visible alterations on the surface of the specimens.

The average color variations ΔE are reported in Table 2. In all cases, the obtained values are lower than the just noticeable difference (JND) fixed to 2.3 [84], which represents the physical threshold under which the human eye cannot perceive color differences. These values are also lower than 1, i.e. an alternative conventional threshold used in literature to identify slightly hue variations (see e.g. [85]), defined as the minimum threshold for 50% color match acceptability [86].

All the ΔE samples are characterized by high coefficients of variation (CoV). These range from 22% to 72% with a mean value equal to 44%, while the corresponding standard deviation values range between 0.11 and 0.30 with a mean value equal to 0.19.

Concerning pull-off tests, for both the aged and the non-aged samples, breaking has always occurred partially inside the base coat (cohesive breaking) and partially at the interface between the base coat and the insulation layer (adhesive breaking, see Fig. 10). From these results, it is clear that the interface between the base coat and insulation layer, as well as the base coat, represents the weakest points of the construction system.

Since the type of finishing coat has not affected the breaking mode, the tensile strengths obtained from the pull-off tests have been grouped by type of base coats and reported in form of box plot (Fig. 11). As it can be seen, each group of non-

aged specimen presents a median failure tension strength of about 0.09-0.10 MPa. This value is slightly higher than the minimum requirement set for similar technologies such as ETICS in reference documents (0.08 MPa [63,64]). Moreover, it should be noted that an increase in bonding strength is obtained due to aging. On average, this increase is about 6.1% for each base coat.

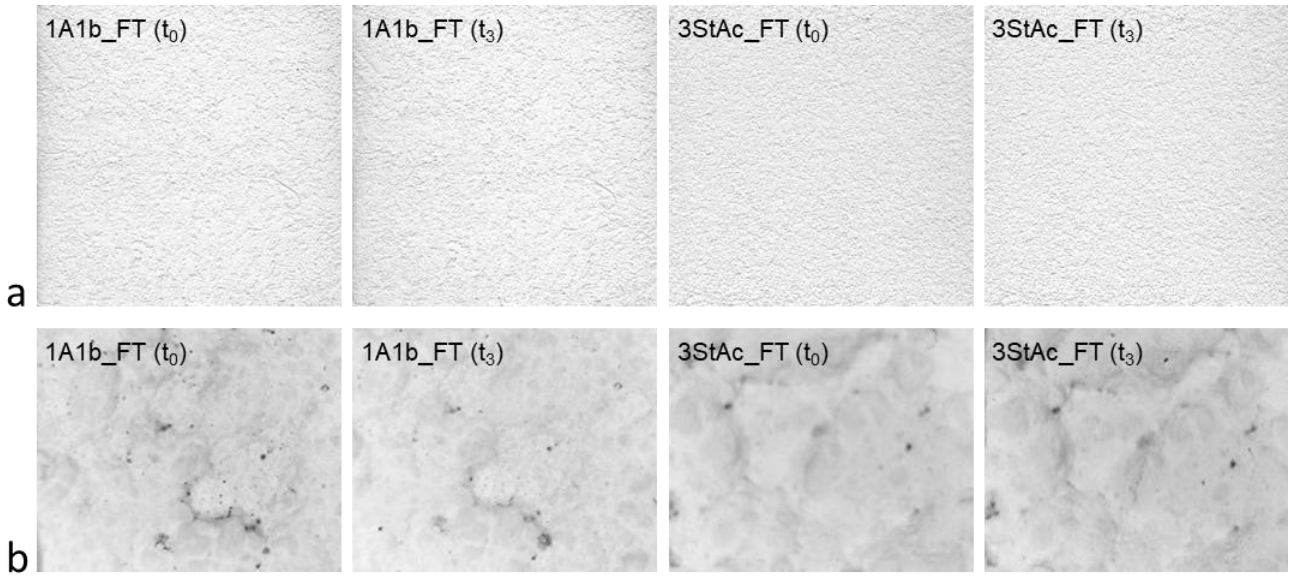

Fig. 9. Examples of digital images taken before (t_0) and after the freeze-thaw test (t_3) for the 1A1*b_FT* and 3StA*c_FT* specimens by using (a) digital scanner and (b) digital microscope.

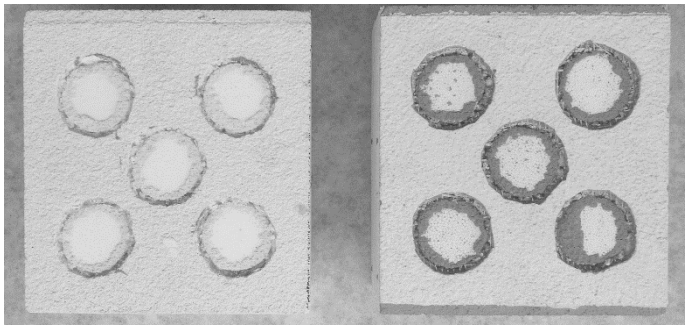

Fig. 10. Example of the failure mode in tensile bond strength tests.

Table 2. Mean color variations (ΔE) of the surface of the specimens calculated at each time interval due to freeze-thaw cycles.

Time interval	Rendering system ID											
	1-AS	*1-A1*	*1-A2*	*1-StA*	*2-AS*	*2-A1*	*2-S*	*2-StA*	*3-AS*	*3-A1*	*3-S*	*3-StA*
t_1	0.48	0.57	0.39	0.50	0.27	0.29	0.34	0.27	0.35	0.28	0.27	0.25
t_2	0.63	0.65	0.40	0.61	0.38	0.49	0.54	0.26	0.45	0.4	0.52	0.27
t_3	0.68	0.65	0.40	0.57	0.43	0.43	0.73	0.27	0.53	0.51	0.74	0.38

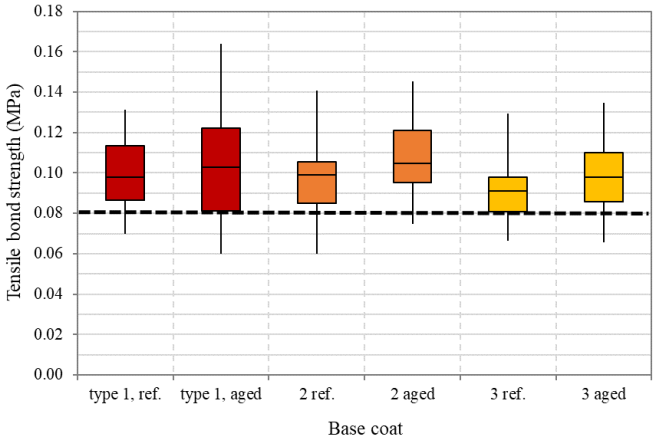

Fig. 11. Tensile bonding strength (MPa) of the rendering system before and after aging through freeze-thaw cycles. Results grouped by type of base coat.

3.3 Wet/drying and UV test

No detachments or other surface alterations due to the accelerated aging process have been observed after visual inspections. However, some slight color variations have been recorded in this case. For each multi-layer rendering system, Fig. 12 reports the average ΔE values computed at each time step. As can be seen, all the rendering systems have shown slight hue variations, i.e. ΔE values higher than 1 [85]. More in detail, according to the JND threshold (ΔE=2.30, [84]), specimens with StA and A2 finishing layers are the only ones that have maintained the original colors, while significant color variations (ΔE>2.30) have been obtained for specimens with the AS, A1 and S finishing coats. In Table 3, the average color variations at the end of the test in terms of CIELab coordinates are reported. From these results, slight variations in L values, corresponding to less bright specimens (negative ΔL), and higher variations in b values, corresponding to less blue and more yellow specimens (positive Δb), can be observed. Concerning the scattering of the results, ΔE samples are characterized by a CoV ranging from 9% to 56% (average value equal to 21%), corresponding to standard deviations ranging from 0.19 to 0.72 (average value equal to 0.37).

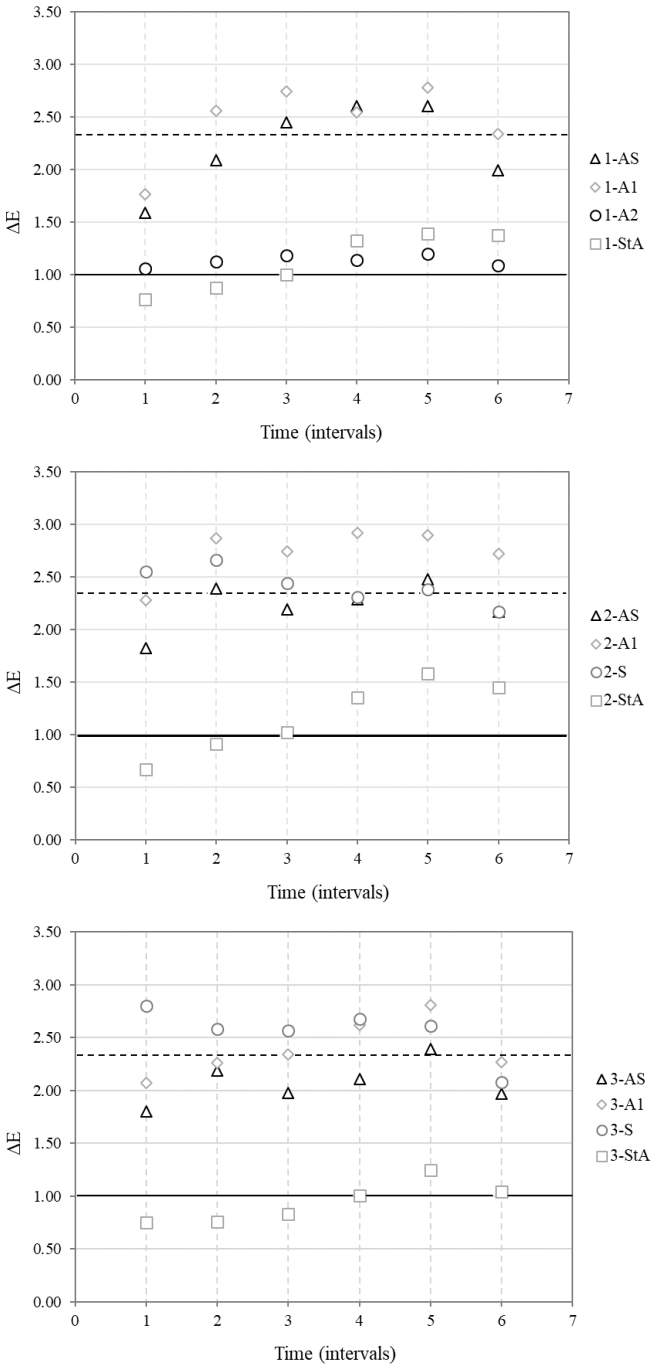

Fig. 12. Mean color variations (ΔE) at each time interval after wet/drying and UV cycles. The horizontal dashed line is the limit under which color differences are not visible to the naked eye (just notable difference JND, ΔE = 2.3 [84]). The horizontal solid line is a conventional threshold used in literature for slight hue variations (ΔE = 1, [85]).

Table 3. Average color variations at the end of the wet/drying and UV test expressed as CIELab color coordinates.

	Multi-layer rendering system ID											
	1-AS	*1-A1*	*1-A2*	*1-StA*	*2-AS*	*2-A1*	*2-S*	*2-StA*	*3-AS*	*3-A1*	*3-S*	*3-StA*
ΔL	-0.86	-0.88	0.20	-0.72	-0.79	-0.73	-0.55	-0.96	-0.84	-0.82	-0.68	-0.56
Δa	-0.09	-0.06	-0.09	-0.03	-0.03	0.02	-0.04	0.01	-0.05	-0.07	-0.08	-0.08
Δb	2.35	2.63	1.23	1.54	2.57	3.35	2.63	1.68	2.27	2.80	2.48	1.20

3.4 ATR-FT-IR analyses on aged samples

Aliquots from the aged samples from both treatments, i.e. freeze-thaw cycles (FT) and UV-wetting cycles (UV), have been investigated by means of ATR-FT-IR spectroscopy as described in section 2.3.2, in order to allow a comparison with the

corresponding non-aged samples. Overall, 15 different multi-layer finishing systems have been analyzed.

As already noted for non-aged samples, all the aged ones have been found to be charged with large quantities of calcium carbonate as a filler (see Fig. 13). For this reason, in order to separate the organic matrix from the calcium carbonate, the overnight extraction with chloroform at room temperature has been carried out even in this case (see Section 3.1.2).

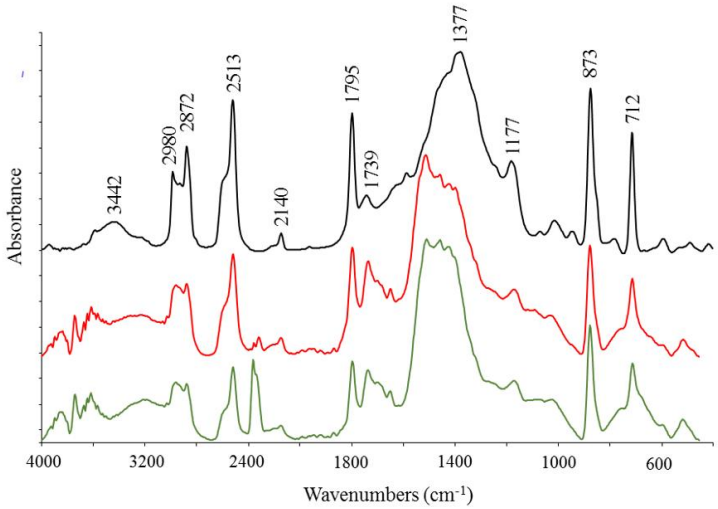

Fig. 13. IR spectra comparison of calcium carbonate alone (black), 2StA_*FT* (red), 2StA_*UV* (green), in the 4000-450 cm^{-1} region.

In Table 4, the results of the analysis carried out in transmission mode on the resulting organic residues from the solvent extraction procedure above described, are reported in terms of most relevant IR peak wavelengths, together with the corresponding vibrational assignments according to the literature, with the main spectral variations arising from both aging treatments in bold [87].

Peak wavenumber (cm^{-1})	Assignment
3322	**Overtone C=C**
3026	**ν =C-H**
2923	ν_{as} CH_2,CH_3
2851	ν_{s} CH_2,CH_3
1730	**ν C=O**
1624	**ν C=C**
1491	δ_{as} CH_2,CH
1451	δ_{s} CH_2,CH_3
1374	**ν COO-**
1260	δ $=CH_2$
1218	γ CH_2,CH_3
1155	γ CH_2,CH_3
1027	ν C-C
906	ν C=C
757	τ CH_2
699	ν C=C

Table 4. Wavenumbers (in cm^{-1}) of the most relevant IR bands in polymeric chains, together with the related vibrational mode marks. **ν**: stretching, **δ**: bending (s: symmetric, as: asymmetric), **γ**: twisting, **τ**: rocking. In bold the main spectral variations arising from both aging treatments.

Considering the organic residues from the solvent extraction procedure above described, the aging effects on the studied systems resulted more evident from the FT-IR study with respect to the findings of the chromatic tests. In particular, the spectral comparison of the organic matrix from the untreated and aged samples showed the typical changes arising from alkyl chains alterations due to incoming oxidative processes. These changes resulted always more evident in the UV-wetting cycles. In

Fig. 14, the spectral comparison of the styrene-acrylic resin 2StA with the corresponding aged ones, 2StA_FT and 2StA_DWUV, has been reported as a typical example.

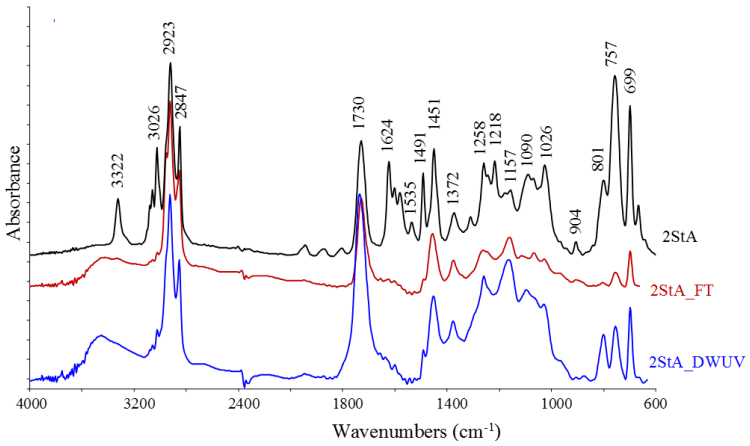

Fig. 14. Comparison between the chloroform extracts representative FT-IR spectrum of the non-aged resin 2StA (black) with those of the aged ones 2StA_FT (red) and 2StA_DWUV (blue).

The IR spectra there reported clearly show some differences arising from aging. In particular, the decreased intensity of the bands at 3026 and 1624 cm^{-1}, attributed to ν(=C-H) and ν(C=C) respectively, with instead an increase of the band at 1730 cm^{-1}, attributed to ν(C=O), because of incoming oxidative processes.

Similar behavior has been found for 2A1. In this case, the changes recorded after aging are more pronounced if compared with 2StA resin, as shown in Fig. 15. In fact, both bands at 3026 and 1624 cm^{-1}, attributed to ν(=C-H) and ν(C=C) respectively, dramatically decreased, together with the increase of the band at 1730 cm^{-1}, attributed to ν(C=O), recording even an inversion of the intensities between the 1624 and 1730 cm^{-1} bands.

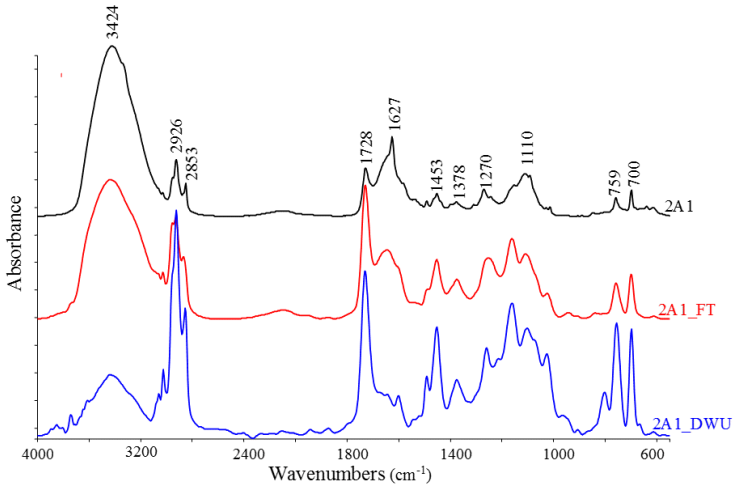

Fig. 15. Comparison between the chloroform extracts representative FT-IR spectrum of the non-aged resin 2A1 (black) with those of the aged ones 2A1_FT (red) and 2A1_DWUV (blue).

Finally, the differences between resin 2S and the corresponding aged ones 2S_FT and 2S_DWUV are shown in Fig. 16. In this case, the organic matrix is represented by an acrylic siloxane resin, hence a different behavior has been observed. However, due to the presence of hydrocarbon chains, changes relative to their aging are present, such as the decrease of bands intensities in the 3300 – 2800 cm^{-1} region (=C-H), also accompanied by the disappearance of the signal at 3322 cm^{-1} attributed to the corresponding overtone. In addition, significant changes occurred in the spectral pattern ranging between 1300 and 1000 cm^{-1}, suggesting that the aging processes deeply affects the resin backbone, where the incoming oxidation process promoted cross-linking and chain scission reactions [88].

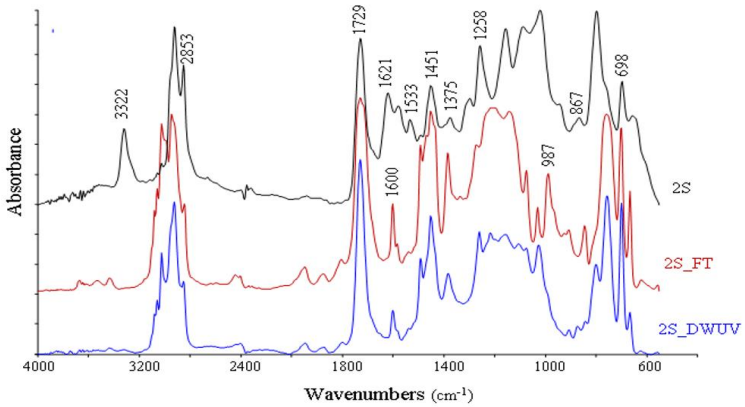

Fig. 16. Comparison between the chloroform extracts representative FT-IR spectrum of the non-aged resin 2S (black) with those of the aged ones 2S_FT (red) and 2S_DWUV (blue).

4 DISCUSSION

The tests carried out in this study have allowed investigating the durability of a reinforced-EPS based construction system in outdoor environments. After aging tests, which have involved the most important atmospheric agents affecting the durability of similar technologies (i.e. thermal shocks, UV radiations and temperature and water content variations), the finishing layers have not shown visible detachments, cracks or other visible defects on the different finishing coats. Then, the presence of the steel wire does not have affected the EPS deformability. This result is similar to that obtained for similar technologies (e.g. [47]), where no visible defects are present on finishing coating after UV cycles. In [47], this was attributed to the presence of TiO_2, able to reduce the transmittance of the UV radiations [89].

Concerning colorimetric analyses, only the wet/drying and UV aging test has caused visible color variations on all the samples. This has been probably due to the UV action that has affected the aesthetic appearance of the external layer, becoming less blue and more yellow [90]. In particular, positive Δb corresponding to a less blue and more yellow specimen, and negative ΔL values, corresponding to a less bright sample, have been obtained for all of the samples, with best results for specimens with StA (styrene-acrylic) and A2 (acrylic) finishing coats. This is similar to that obtained in [91], where a positive Δb and a negative ΔL of a white siloxane finishing coat applied on a reinforced concrete slate were obtained after four years of natural exposure in Milan, Italy. In particular, in [91] a stable value of Δb of approximately 3 was reached after aging. This value is comparable to that obtained in our work at the end of accelerated tests, ranging between 2.3 and 3.3 for the acrylic and acrylic siloxane resins. Conversely, ΔL values are less comparable. In fact, in [91] a ΔL value equal to -15 was obtained after the natural exposure in the urban environment, which is much higher than those obtained in our study (i.e. between -0.5 and -1). The obtained higher values can be attributable to the absence of pollution and dirt in the accelerated tests that, instead, are massively present in urban environments.

The tensile bond strength results indicate the good mechanical performance of the composite system before and after aging processes. In fact, the obtained tensile strengths values are higher than 0.8 MPa (i.e. the minimum requirement sets for ETICS in reference documents [63,64]). An increase of the tensile strength has been also registered after the aging process, probably due to the curing of the base coat during aging cycles. The breaking mode has not varied after the aging test. In particular, a mixed-mode has been obtained in all of the cases, with fracture lines developing inside the base coat between glass fiber mesh and the insulation layer, and at the interface between the base coat and insulation layer. This implies that the joints between the external multi-layer rendering system and reinforced-EPS panels, as well as the base coat, represents the weakest points of the construction system.

Finally, the FT-IR spectral variations observed after both aging treatments are diagnostic of autooxidative processes, which are more evident in UV cycles as expected in processes involving organic free radicals.

In fact, molecular oxygen plays an important role in aging and represents the main responsible of the olefin (C=C and C=C-H) moieties transformation in the organic polymeric fraction of the samples under investigation. In particular, these moieties are converted into the corresponding oxidation products characterized by the presence of carbonyl (C=O) moieties. In terms of IR spectra, this behavior produces the observed intensity decrease of the bands present in the region between 3300 – 2800 cm^{-1} as well as at 1624 cm^{-1}, typical of the C=C and C=C-H moieties, accompanied by an increased intensity of the C=O band at 1730 cm^{-1}, due to the formation of carbonyl derivatives, such as aldehydes, lactones and ketones, typical of hydrocarbon polymer chains oxidative degradation. In the styrene-acrylic resin 2StA, these changes occur to a minor extent, probably for a less reactivity due to the presence of the styrene moiety. On the other hand, siloxanes are known to be less reactive toward molecular oxygen, and the aging process behaves differently. In the acryl siloxane resin 2S, the hydrocarbon (acrylic) component follows the mechanism described above, while the siloxane one mainly undergoes cross-linking and chain scission reactions responsible of polymer backbone alterations, according to the significant changes observed in the spectral pattern in the IR region between 1300 and 1000 cm^{-1}.

However, all the specimens seem to resist satisfactorily to weathering actions.

5 CONCLUSIONS

In this study, the durability in the outdoor environment of a novel reinforced-EPS based construction system named HOMEDONE, developed for affordable and temporary housing solutions, has been investigated.

The results of this experimental campaign, which represents the initial stage of a wider research program on the hygrothermal performance of HOMEDONE panels, have pointed out the absence of significant defects on different external finishing layers after freeze-thaw cycles and wet/drying and UV cycles. After freeze-thaw cycles, pull-off tests results have shown good mechanical performance, even higher than the limits fixed by reference standards for ordinary ETICS with render finishing [63,64]. After wet/drying and UV cycles, some color variations have been recorded, with the best results obtained for specimens with styrene-acrylic and acrylic finishing coats. These results are comparable with those obtained for a siloxane finishing coat exposed for four years to the urban environment.

In addition, the present study indicates FT-IR spectroscopy as a powerful tool to investigate the incoming of degradation processes, even occurring to a small extent, due to its sensitivity with respect to chromatic tests, also allowing to evaluate the aging processes at a molecular level. Even in this case, the styrene-acrylic resin showed minor changes than other resins, probably due to the less reactivity caused by the presence of the styrene moiety.

In conclusion, the results obtained in this study indicate the HOMEDONE construction system as a promising and durable solution for affordable housing and emergency shelter. The thermal and hygrothermal behavior of such a system will be investigated in a further stage of the research.

6 ACKNOWLEDGMENTS

Financial support for this study was provided by the AC-Engineering S.p.A under the "POR FESR Marche 2014/2020" Research Project No. 15345.

7 REFERENCES

[1] P. Berdahl, H. Akbari, R. Levinson, W.A. Miller, Weathering of roofing materials-An overview, (2006). doi:10.1016/j.conbuildmat.2006.10.015.

[2] C.Y. Yiu, D.C.W. Ho, S.M. Lo, Weathering effects on external wall tiling systems, Constr. Build. Mater. 21 (2007) 594–600. doi:10.1016/j.conbuildmat.2005.11.002.

[3] J. Bochen, Weathering effects on physical–chemical properties of external plaster mortars exposed to different environments, Constr. Build. Mater. 79 (2015) 192–206. doi:10.1016/j.conbuildmat.2014.12.079.

[4] J. Souza, A. Silva, J. de Brito, E. Bauer, Service life prediction of ceramic tiling systems in Brasília-Brazil using the factor method, Constr. Build. Mater. 192 (2018) 38–49. doi:10.1016/j.conbuildmat.2018.10.084.

[5] J. Bochen, Study on the microstructure of thin-layer facade plasters of thermal insulating system during artificial weathering, Constr. Build. Mater. 23 (2009) 2559–2566. doi:10.1016/j.conbuildmat.2009.02.028.

[6] J. Bochen, S. Gil, Properties of pore structure of thin-layer external plasters under ageing in simulated environment, Constr. Build. Mater. 23 (2009) 2958–2963. doi:10.1016/j.conbuildmat.2009.02.041.

[7] N.L. Alchapar, E.N. Correa, Aging of roof coatings. Solar reflectance stability according to their morphological characteristics, Constr. Build. Mater. 102 (2016) 297–305. doi:10.1016/j.conbuildmat.2015.11.005.

[8] E. Franzoni, B. Pigino, G. Graziani, C. Lucchese, A. Fregni, A new prefabricated external thermal insulation composite board with ceramic finishing for buildings retrofitting, Mater. Struct. 49 (2016) 1527–1542. doi:10.1617/s11527-015-0593-7.

[9] A. Vilhena, C. Silva, P. Fonseca, S. Couto, Exterior walls covering system to improve thermal performance and increase service life of walls in rehabilitation interventions, Constr. Build. Mater. 142 (2017) 354–362. doi:10.1016/j.conbuildmat.2017.03.033.

[10] X. Gan, J. Zuo, P. Wu, J. Wang, R. Chang, T. Wen, How affordable housing becomes more sustainable? A stakeholder study, J. Clean. Prod. 162 (2017) 427–437. doi:10.1016/j.jclepro.2017.06.048.

[11] H. Wallbaum, Y. Ostermeyer, C. Salzer, E. Zea Escamilla, Indicator based sustainability assessment tool for affordable housing construction technologies, Ecol. Indic. 18 (2012) 353–364. doi:10.1016/j.ecolind.2011.12.005.

[12] Eurostat, Migration and migrant population statistics - Statistics Explained, (2018). http://ec.europa.eu/eurostat/statistics-explained/index.php/Migration_and_migrant_population_statistics (accessed December 27, 2017).

[13] Centre for Research on the Epidemiology of Disasters (CRED), The international disasters database, (2017). http://www.emdat.be/ (accessed December 27, 2017).

[14] S.M. Amin Hosseini, A. De La Fuente, O. Pons, Multi-criteria decision-making method for assessing the sustainability of post-disaster temporary housing units technologies: A case study in Bam, 2003, Sustain. Cities Soc. 20 (2016) 38–51. doi:10.1016/j.scs.2015.09.012.

[15] A. Atmaca, N. Atmaca, Comparative life cycle energy and cost analysis of post-disaster temporary housings, Appl. Energy. 171 (2016) 429–443. doi:10.1016/j.apenergy.2016.03.058.

[16] J. Woetzel, S. Ram, J. Mischke, N. Garemo, S. Sankhe, A blueprint for addressing the global affordable housing challenge, McKinsey&Company, 2014.

[17] UN-Habitat, United Nations Human Settlements Programme, (n.d.). https://unhabitat.org/ (accessed December

21, 2017).
[18] J. Woetzel, S. Ram, S. Peloquin, M. Limam, J. Mischke, Housing affordability: A supply-side tool kit for cities, McKinsey&Company, 2017.
[19] S.J. Kolo, F.P. Rahimian, J.S. Goulding, Offsite manufacturing construction: A big opportunity for housing delivery in Nigeria, Procedia Eng. 85 (2014) 319–327. doi:10.1016/j.proeng.2014.10.557.
[20] J. Woetzel, J. Mischke, S. Peloquin, D. Weisfield, A tool kit to close california's housing gap: 3.5 million homes by 2025, McKinsey&Company, 2016.
[21] UNRWA - United Nations Relief and Works Agency for Palestine refugees in the near east, Palestine refugees | UNRWA, (n.d.). https://www.unrwa.org/palestine-refugees (accessed September 19, 2018).
[22] R. Thapa, H.B. Rijal, M. Shukuya, Field study on acceptable indoor temperature in temporary shelters built in Nepal after massive earthquake 2015, Build. Environ. 135 (2018) 330–343. doi:10.1016/j.buildenv.2018.03.001.
[23] UNHCR - The UN Refugee Agency, UNHCR - Figures at a Glance. Statistical yearbooks, (2019). http://www.unhcr.org/uk/figures-at-a-glance.html (accessed September 19, 2018).
[24] IDMC, Global Internal Displacement Database | IDMC, (2019). http://www.internal-displacement.org/database (accessed September 19, 2019).
[25] IDMC, GRID 2018 | Global Report on Internal Displacement 2018, (2018). http://internal-displacement.org/global-report/grid2018/ (accessed September 19, 2019).
[26] F. Barbosa, J. Woetzel, J. Mischke, M.J. Ribeirinho, M. Sridhar, M. Parsons, N. Bertram, S. Brown, Reinventing Construction: A Route To Higher Productivity, McKinsey&Company, 2017.
[27] H.M. Bernstein, E.J. Gudjel, D. Laquidara-Carr, Prefabrication and Modularization: Increasing Productivity in the Construction Industry, McGraw-Hill Construction, 2011.
[28] N. Lu, The current use of offsite construction techniques in the united states construction industry, in: 2009 Constr. Res. Congr., 2009. doi:10.1061/41020(339)96.
[29] R.M. Lawson, R.G. Ogden, Sustainability and Process Benefits of Modular Construction, 8th CIB World Build. Congr. (2010).
[30] E.M. Generalova, V.P. Generalov, A.A. Kuznetsova, Modular Buildings in Modern Construction, in: Procedia Eng., 2016. doi:10.1016/j.proeng.2016.08.098.
[31] D. Lopez, T.M. Froese, Analysis of Costs and Benefits of Panelized and Modular Prefabricated Homes, Procedia Eng. 145 (2016) 1291–1297. doi:10.1016/j.proeng.2016.04.166.
[32] R.M. Lawson, R.G. Ogden, R. Bergin, Application of Modular Construction in High-Rise Buildings, J. Archit. Eng. (2012). doi:10.1061/(ASCE)AE.1943-5568.0000057.
[33] X.X. Li, G.L. Li, Exploration of Modular Build of Architectural Space, Appl. Mech. Mater. (2013). doi:10.4028/www.scientific.net/AMM.357-360.338.
[34] G. Tumminia, F. Guarino, S. Longo, M. Ferraro, M. Cellura, V. Antonucci, Life cycle energy performances and environmental impacts of a prefabricated building module, Renew. Sustain. Energy Rev. 92 (2018) 272–283. doi:10.1016/j.rser.2018.04.059.
[35] L. Aye, T. Ngo, R.H. Crawford, R. Gammampila, P. Mendis, Life cycle greenhouse gas emissions and energy analysis of prefabricated reusable building modules, Energy Build. 47 (2012) 159–168. doi:10.1016/j.enbuild.2011.11.049.
[36] D. Albadra, D. Coley, J. Hart, Toward healthy housing for the displaced, J. Archit. 23 (2018) 115–136. doi:10.1080/13602365.2018.1424227.
[37] Y. Wang, L. Wang, E. Long, S. Deng, An experimental study on the indoor thermal environment in prefabricated houses in the subtropics, Energy Build. 127 (2016) 529–539. doi:10.1016/j.enbuild.2016.05.061.
[38] L. Huang, E. Long, J. Ouyang, Measurement of the Thermal Environment in Temporary Settlements with High Building Density after 2008 Wenchuan Earthquake in China, Procedia Eng. 121 (2015) 95–100. doi:10.1016/j.proeng.2015.08.1027.
[39] M. Košir, N. Iglič, R. Kunič, Optimisation of heating, cooling and lighting energy performance of modular buildings in respect to location's climatic specifics, Renew. Energy. 129 (2018) 527–539. doi:10.1016/j.renene.2018.06.026.
[40] P. Samani, V. Leal, A. Mendes, N. Correia, Comparison of passive cooling techniques in improving thermal comfort of occupants of a pre-fabricated building, Energy Build. 120 (2016) 30–44. doi:10.1016/j.enbuild.2016.03.055.
[41] F. Barreca, V. Tirella, A self-built shelter in wood and agglomerated cork panels for temporary use in Mediterranean climate areas, Energy Build. 142 (2017) 1–7. doi:10.1016/j.enbuild.2017.03.003.
[42] D. Rockwood, J.T. da Silva, S. Olsen, I. Robertson, T. Tran, Design and prototyping of a FRCC modular and climate responsive affordable housing system for underserved people in the pacific island nations, J. Build. Eng. 4 (2015) 268–282. doi:10.1016/j.jobe.2015.09.013.
[43] P. Cherian, S. Paul, S.R.G. Krishna, D. Menon, A. Meher Prasad, Mass Housing Using GFRG Panels: A Sustainable, Rapid and Affordable Solution, J. Inst. Eng. Ser. A. 98 (2017) 95–100. doi:10.1007/s40030-017-0200-8.
[44] A.S. Sferra, Emergency: innovative prefabricated construction components for an eco-solidarity architecture, TECHNE - J. Technol. Archit. Environ. (2017) 328–334. doi:10.13128/Techne-20788.
[45] S. Ximenes, J. de Brito, P.L. Gaspar, A. Silva, Modelling the degradation and service life of ETICS in external walls,

Mater. Struct. 48 (2015) 2235–2249. doi:10.1617/s11527-014-0305-8.
[46] R. NORVAIŠIENĖ, G. GRICIUTĖ, R. BLIŪDŽIUS, J. RAMANAUSKAS, The Changes of Moisture Absorption Properties during the Service Life of External Thermal Insulation Composite System, Mater. Sci. 19 (2013) 103–107. doi:10.5755/j01.ms.19.1.3834.
[47] G. Griciutė, R. Bliūdžius, Study on the microstructure and water absorption rate changes of exterior thin-layer polymer renders during natural and artificial ageing, Medziagotyra. 21 (2015) 149–154. doi:10.5755/j01.ms.21.1.4869.
[48] B. Daniotti, R. Paolini, F. Re Cecconi, Effects of Ageing and Moisture on Thermal Performance of ETICS Cladding, in: V.P. de de Freitas, J.M.P.Q. Delgado (Eds.), Springer Berlin Heidelberg, Berlin, Heidelberg, 2013: pp. 127–171. doi:10.1007/978-3-642-37475-3_6.
[49] B. Daniotti, F.R. Cecconi, R. Paolini, R. Galliano, J. Ferrer, L. Battaglia, Durability evaluation of ETICS: analysis of failures case studies and heat and moisture transfer simulations to assess the frequency of critical events, in: 4th Port. Conf. Mortars ETICS, 2012.
[50] J. Šadauskienė, V. Stankevičius, R. Bliūdžius, A. Gailius, The impact of the exterior painted thin-layer render's water vapour and liquid water permeability on the moisture state of the wall insulating system, Constr. Build. Mater. 23 (2009) 2788–2794. doi:10.1016/J.CONBUILDMAT.2009.03.010.
[51] T. Kvande, N. Bakken, E. Bergheim, J.V. Thue, T. Kvande, N. Bakken, E. Bergheim, J.V. Thue, Durability of ETICS with Rendering in Norway—Experimental and Field Investigations, Buildings. 8 (2018) 93. doi:10.3390/buildings8070093.
[52] S.S. de Freitas, V.P. de Freitas, Cracks on ETICS along thermal insulation joints: case study and a pathology catalogue, Struct. Surv. 34 (2016) 57–72. doi:10.1108/SS-09-2015-0043.
[53] H. Shen, H. Tan, A. Tzempelikos, The effect of reflective coatings on building surface temperatures, indoor environment and energy consumption - An experimental study, Energy Build. 43 (2011) 573–580. doi:10.1016/j.enbuild.2010.10.024.
[54] E. Barreira, V.P. De Freitas, Experimental study of the hygrothermal behaviour of External Thermal Insulation Composite Systems (ETICS), Build. Environ. 63 (2013) 31–39. doi:10.1016/j.buildenv.2013.02.001.
[55] H. Xiong, J. Xu, Y. Liu, S. Wang, Experimental Study on Hygrothermal Deformation of External Thermal Insulation Cladding Systems with Glazed Hollow Bead, Adv. Mater. Sci. Eng. 2016 (2016) 1–14. doi:10.1155/2016/3025213.
[56] B. Amaro, D. Saraiva, J. De Brito, I. Flores-Colen, Inspection and diagnosis system of ETICS on walls, Constr. Build. Mater. 47 (2013) 1257–1267. doi:10.1016/j.conbuildmat.2013.06.024.
[57] J.A.R. Mendes Silva, J. Falorca, A model plan for buildings maintenance with application in the performance analysis of a composite facade cover, Constr. Build. Mater. 23 (2009) 3248–3257. doi:10.1016/j.conbuildmat.2009.05.008.
[58] S.H. Ding, D.Z. Liu, Durability evaluation of building sealants by accelerated weathering and thermal analysis, Constr. Build. Mater. 20 (2006) 878–881. doi:10.1016/j.conbuildmat.2005.06.026.
[59] M. Lopes, V. Mouillet, L. Bernucci, T. Gabet, The potential of Attenuated Total Reflection imaging in the mid-infrared for the study of recycled asphalt mixtures, Constr. Build. Mater. 124 (2016) 1120–1131. doi:10.1016/j.conbuildmat.2016.08.108.
[60] L.D. Poulikakos, S. dos Santos, M. Bueno, S. Kuentzel, M. Hugener, M.N. Partl, Influence of short and long term aging on chemical, microstructural and macro-mechanical properties of recycled asphalt mixtures, Constr. Build. Mater. 51 (2014) 414–423. doi:10.1016/j.conbuildmat.2013.11.004.
[61] F. Iucolano, D. Caputo, F. Leboffe, B. Liguori, Mechanical behavior of plaster reinforced with abaca fibers, Constr. Build. Mater. 99 (2015) 184–191. doi:10.1016/j.conbuildmat.2015.09.020.
[62] M. D'Orazio, G. Maracchini, An experimental investigation on the indoor hygrothermal environment of a reinforced-EPS based temporary housing solution, Energy Build. 204 (2019) 109500. doi:10.1016/j.enbuild.2019.109500.
[63] European Organisation for Technical Approvals (EOTA), ETAG 004 - Guidelines for European Technical Approval of External Thermal Insulation Composite Systems (ETICS) With Rendering, 2013.
[64] CEN, EN 13499:2005, Thermal insulation products fo building - external thermal insulation composite systems (ETICS) based on expanded polystyrene - specification, 2005.
[65] ASTM, ASTM E 2110-11 Standard terminology for exterior insulation and finish systems (EIFS), 2011.
[66] EN 13687-4 Products and systems for the protection and repair of concrete structures - Test method - Determination of thermal compatibility - Dry thermal cycling, (2002).
[67] ISO 16474-3:2013. Paints and varnishes - Methods of exposure to laboratory light sources Fluorescent UV lamps, (2013).
[68] T. Uygunoğlu, S. Özgüven, M. Çalış, Effect of plaster thickness on performance of external thermal insulation cladding systems (ETICS) in buildings, Constr. Build. Mater. 122 (2016) 496–504. doi:10.1016/j.conbuildmat.2016.06.128.
[69] D. Félix, D. Monteiro, J.M. Branco, R. Bologna, A. Feio, The role of temporary accommodation buildings for post-disaster housing reconstruction, J. Hous. Built Environ. 30 (2014) 683–699. doi:10.1007/s10901-014-9431-4.
[70] (CEN) European Committee for Standardisation, EN 10027-1: 2005 Designation systems for steels - Part 1: Steel

names, Eur. Stand. 3 (2005) 1–25.
[71] D. Félix, J.M. Branco, A. Feio, Temporary housing after disasters: A state of the art survey, Habitat Int. 40 (2013) 136–141. doi:10.1016/j.habitatint.2013.03.006.
[72] F. Barreca, C.R. Fichera, Thermal insulation performance assessment of agglomerated cork boards, Wood Fiber Sci. 48 (2016) 96–103.
[73] F. Barreca, G. Modica, S. Di Fazio, V. Tirella, R. Tripodi, C.R. Fichera, Improving building energy modelling by applying advanced 3D surveying techniques on agri-food facilities, J. Agric. Eng. 48 (2017) 203–208. doi:10.4081/jae.2017.677.
[74] E. Lucchi, Applications of the infrared thermography in the energy audit of buildings: A review, Renew. Sustain. Energy Rev. (2018). doi:10.1016/j.rser.2017.10.031.
[75] A.M. Tanyer, A. Tavukcuoglu, M. Bekboliev, Assessing the airtightness performance of container houses in relation to its effect on energy efficiency, Build. Environ. 134 (2018) 59–73. doi:10.1016/j.buildenv.2018.02.026.
[76] Y. Govaerts, R. Hayen, M. de Bouw, A. Verdonck, W. Meulebroeck, S. Mertens, Y. Grégoire, Performance of a lime-based insulating render for heritage buildings, Constr. Build. Mater. (2018). doi:10.1016/j.conbuildmat.2017.10.115.
[77] EN 1504-3:2006. Products and systems for the protection and repair of concrete structures. Definitions, requirements, quality control and evaluation of conformity. Part 3: Structural and non-structural repair, (2006).
[78] EN ISO 4628-1:2016. Paint and varnishes - Evaluation of degradation of coatings - Designation of quantity and size of defects, and of intensity of uniform changes in appearance - Part 1: General introduction and designation system, (2016).
[79] ISO/CIE 11664-6:2014. Colorimetry - Part 6: CIEDE 2000 Colour difference formula, (2014).
[80] EN 1542:1999. Products and systems for the protection and repair of concrete structures - Test methods - Measurement of bond strength by pull-off, (1999).
[81] EN 1062-11:2002. Paints and varnishes - Coating materials and coating systems for exterior masonry and concrete - Part 11: Methods of conditioning before testing, (2002).
[82] ISO 16474-1:2013. Paints and varnishes -- Methods of exposure to laboratory light sources General guidance, (2013).
[83] J. Lanas, J.L. Pérez Bernal, M.A. Bello, J.I. Alvarez, Mechanical properties of masonry repair dolomitic lime-based mortars, Cem. Concr. Res. (2006). doi:10.1016/j.cemconres.2005.10.004.
[84] G. Sharma, Digital color imaging handbook, CRC Press, 2003.
[85] E. Quagliarini, F. Bondioli, G.B. Goffredo, A. Licciulli, P. Munafò, Smart surfaces for architectural heritage: Preliminary results about the application of TiO2-based coatings on travertine, J. Cult. Herit. 13 (2012) 204–209. doi:10.1016/j.culher.2011.10.002.
[86] R.G. Kuehni, R.T. Marcus, An Experiment in Visual Scaling of Small Color Differences, Color Res. Appl. (1979). doi:10.1111/j.1520-6378.1979.tb00094.x.
[87] T. Gocen, S.H. Bayari, M.H. Guven, Conformational and vibrational studies of arachidonic acid, light and temperature effects on ATR-FTIR spectra, Spectrochim. Acta - Part A Mol. Biomol. Spectrosc. (2018). doi:10.1016/j.saa.2018.05.100.
[88] N.S. Tomer, F. Delor-Jestin, L. Frezet, J. Lacoste, Oxidation, Chain Scission and Cross-Linking Studies of Polysiloxanes upon Ageings, Open J. Org. Polym. Mater. 02 (2012) 13–22. doi:10.4236/ojopm.2012.22003.
[89] H. Fjellstrom, H. Hoglund, S. Forsberg, M. Paulsson, The UV-screening properties of coating layers: The influence of pigments, binders and additives, Nord. Pulp Pap. Res. J. 24 (2009) 206–212. doi:10.3183/NPPRJ-2009-24-02-p206-212.
[90] S. Cabral-Fonseca, J.R. Correia, M.P. Rodrigues, F.A. Branco, Artificial accelerated ageing of GFRP pultruded profiles made of polyester and vinylester resins: Characterisation of physical-chemical and mechanical damage, Strain. 48 (2012) 162–173. doi:10.1111/j.1475-1305.2011.00810.x.
[91] R. Paolini, A. Zani, T. Poli, F. Antretter, M. Zinzi, Natural aging of cool walls: Impact on solar reflectance, sensitivity to thermal shocks and building energy needs, Energy Build. 153 (2017) 287–296. doi:10.1016/j.enbuild.2017.08.017.

DETAILED RESPONSE TO REVIEWERS

We have greatly appreciated the reviewer's efforts in carefully reviewing the paper. Thus, we thank them for their deep and thorough review. We have revised the paper according to their suggestions and comments, and we hope to have accomplished all their requests. All the corrections and new texts are reported in red in the manuscript.
Number wise answers to their specific comments/suggestions/queries are reported in the following.

1 Response to Reviewer #1' Comments

General comment: This paper reports a comprehensively experimental study of the durability of a prefabricated reinforced EPS based panel. Various environmental factors were considered: freeze-thaw, wet/drying-UV aging. Several techniques were used to evaluate the panels after exposed to those environmental conditions. The testings and results are clearly described.

Comment #1: However, all tests are tied to one industrial product. The in-depth theoretical analysis is desired in order to extend the findings from this research to broader applications.

Response #1: Thank you for this remark that has allowed us to enhance the quality of the paper. In order to allow extending the obtained results to broader applications, a "Material characterization" Section has been added to the paper (see Section 2.1 and 3.1). X-ray diffraction (XRD) analyses on powered samples of hydrated base coats have been carried out to characterize the adopted base coat materials. The ATR-FTIR analyses are instead used to characterize the finishing coat materials. The main XRD results added to the paper are reported in the following:

"As expected, the diffraction bands show the presence of cement binder components like alite and calcite in all the analyzed materials, as observed for similar thin-layer plaster typically applied on EPS or cement substrates (see e.g. [5]). The basecoats mainly differ from each other due to the use of different types of sand filler. In particular, for basecoats 1 and 2, the most often detected peak is related to quartz that, along with mica, chlorite and natural silicates, indicates the use of natural silica sand filler for manufacturing the two mortars [5]. Differently, for basecoat 3, the presence of ankerite is observed, denoting the use of carbonate sand instead of silica sand [83]."

2 Response to Reviewer #2' Comments

General comment: The main aim, in this work, the thermal compatibility among the different layers of the HOMEDONE construction system is investigated with appropriate accelerated aging tests, i.e. freeze-thaw tests and wet/drying and UV tests. These tests involve the most relevant atmospheric agents affecting the durability of EPS walls with multilayer rendering systems, such as thermal shocks, UV radiation and variations in water contents (driving rain), excepting for physical and chemical agents such as pollutants that have been not considered in this study. During tests, the development of cracking, detachments and variations in bonding strength between different layers have been then measured. Fourier Transform Infrared (FT-IR) spectroscopic analyses have been also carried out in order to understand the effects of aging processes on a micro scale. The paper is well done but I have some remarks:

Comment #1: The authors should explain better the thermal performance variation of the entire module (some references: Improving building energy modelling by applying advanced 3D surveying techniques on agri-food facilities, Thermal insulation performance assessment of agglomerated cork boards, ecc).

Response #1: Thank you for this remark that allows us to enhance the quality of the paper. Actually, the experimental investigation carried out in the study is focused on the single HOMEDONE panel, while experimental and numerical investigations on the entire module, including its thermal performance, have been considered in recent studies (see e.g. [62]). However, in order to explain better the thermal performance variation of the single HOMEDONE panel, a thermographic analysis has been added to this work, and the following sentences have been added in Section 2.2:

"Before carrying out aging tests, qualitative and quantitative information on the thermal performance variation of the chosen panel due to the presence of the embedded steel bars have been collected. In particular, first a qualitative

*estimation of the surface temperatures variation on the panel surface was obtained through an active infrared thermographic analysis on a panel purposely heated at 55°C [72–74]. At this aim, a Mikron 7800 Infrared Camera was used, while climatic data, emissivity value (set equal to 0.95 [75]) and the distance of the thermal camera from the target area were set up into the NRG Pro software v.1.997 to obtain a good estimation of the temperatures. Then, in order to evaluate the thermal performance variation of a panel in real use conditions, surface temperatures and heat fluxes were measured in different points of a real panel used to build an experimental mock-up (see [62]). As a result, the IR camera showed a temperature difference on the panel surface of about 0.25°C when the IR photo was taken (**Error! Reference source not found.**). The in situ survey showed no significant variations between the measured surface temperatures and between heat fluxes, denoting a sufficiently good homogeneity of the panel in terms of thermal performance in real use conditions [62].".*

Comment #2: There are some unit measure errors (e.g. row 151, ecc.).

Response #2: Thank you. Unit measures have been corrected throughout the text.

HIGHLIGHTS

- The durability of an EPS-based construction system (HOMEDONE) is investigated;
- EPS-panel are internally reinforced with a 3D metal grid;
- Freeze-thaw and wet/drying and UV tests are carried out;
- The aging processes are investigated through FT-IR spectroscopy;
- HOMEDONE is a durable option for affordable and temporary housing solution.

***Declaration of Interest Statement**

Declaration of interests

☒ The authors declare that they have no known competing financial interests or personal relationships that could have appeared to influence the work reported in this paper.

☐The authors declare the following financial interests/personal relationships which may be considered as potential competing interests:

CRediT authors statement

Marco D'Orazio: Conceptualization, Methodology, Validation, Resources, Writing – review and editing, Supervision, Project administration, Funding acquisition

Pierluigi Stipa: Methodology, Formal analysis, Resources, Writing – review and editing

Simona Sabbatini: Methodology, Validation, Formal analysis, Investigation, Data curation, Writing – original draft, Visualization

Gianluca Maracchini: Methodology, Validation, Formal Analysis, Investigation, Data curation, Writing – original draft, Writing – review and editing, Visualization, Project administration

*Title page

Experimental investigation on the durability of a novel lightweight prefabricated Reinforced-EPS based construction system

M. D'Orazio[a], P. Stipa[b], S. Sabbatini[c], G. Maracchini[d]*

[a] Department of Civil and Building Engineering and Architecture (DICEA), Polytechnic University of Marche, via Brecce Bianche, 60131, Ancona, Italy, email: m.dorazio@staff.univpm.it

[b] Department of Materials, Environmental Sciences and Urban Planning (SIMAU), Polytechnic University of Marche, via Brecce Bianche, 60131, Ancona, Italy, email: p.stipa@staff.univpm.it

[c] Department of Materials, Environmental Sciences and Urban Planning (SIMAU), Polytechnic University of Marche, via Brecce Bianche, 60131, Ancona, Italy, s.sabbatini@staff.univpm.it

[d*] Department of Civil and Building Engineering and Architecture (DICEA), Polytechnic University of Marche, via Brecce Bianche, 60131, Ancona, Italy, email: g.maracchini@staff.univpm.it (Corresponding author)

Experimental investigation on the durability of a novel lightweight prefabricated Reinforced-EPS based construction system

M. D'Orazio[a], P. Stipa[b], S. Sabbatini[b], G. Maracchini[a]*

[a] Department of Civil and Building Engineering and Architecture (DICEA), Polytechnic University of Marche, via Brecce Bianche, 60131, Ancona, Italy
[b] Department of Materials, Environmental Sciences and Urban Planning (SIMAU), Polytechnic University of Marche, via Brecce Bianche, 60131, Ancona, Italy

*corresponding author. *E-mail address*: g.maracchini@staff.univpm.it
E-mail addresses: m.dorazio@staff.univpm.it; p.stipa@univpm.it; s.sabbatini@univpm.it; g.maracchini@staff.univpm.it

ABSTRACT

This paper investigates the durability of a low-cost construction system named HOMEDONE developed to realize affordable and also temporary housing solutions. The system is based on the assembly of 3D-reinforced EPS panels externally topped off with a multi-layer rendering system. Similar technologies showed durability issues, especially in hot climates, due to the thermal and hygrometric stresses of the thin finishing layers when coupled to thick EPS panels and exposed to extreme events. For this reason, in this work freeze-thaw and wet/drying-UV aging tests on HOMEDONE panels with different finishing systems have been carried out, monitoring macroscopic, microscopic (ATR-FT-IR analysis) and bond strength variations due to aging. Results have pointed out good mechanical properties of the system and only small color variations of the finishing layer due to UV cycles. Then, HOMEDONE can be considered as a durable option for affordable and temporary housing solutions.

KEYWORDS

Affordable housing; Temporary housing; Reinforced EPS; Prefabricated; Durability; Pull-off; ATR-FT-IR spectroscopy; XRD analysis

1 INTRODUCTION

Durability is one of the most important criteria for materials selection in building constructions. The natural deterioration of building components, in fact, leads to a loss of performance of these elements, affecting their original characteristics and compromising the fulfillment of specific requirements during building service life.

Roofs and external walls are the building components most affected by durability issues since directly exposed to the most aggressive actions (climate, impact, etc.) [1–3]. These elements, however, have also important functions such as protection, thermal insulation and watertightness, which must be guaranteed for a specified minimum period of time [4]. Then, it is important to investigate their durability, suitability for use and aging processes, even in order to optimize the adoption of preventive and effective interventions.

With this aims, a lot of studies in literature investigated the durability of traditional roof and walls components, mainly focusing on the behavior under extreme environmental conditions of their covering materials, such as mortars, ceramic tiles, natural stone, ETICS, wood panels, curtain walls and ventilated façades (see e.g. [1–3,5–9]).

However, the increasing global need of affordable housing [10,11] and temporary accommodations for post-disaster scenarios (increasingly frequent due to climate change [12,13]) are pushing the research towards the development of new and non-traditional low-cost building components, whose durability is often treated as a secondary aspect [14,15]. In particular, about 330 million urban households around the world live today in inadequate housing or are financially overstretched by housing costs [16–18] and 106 million additional households, i.e. about 1.6 billion additional people, will face the affordability challenge in 2025 [16,19,20]. In addition, over 60 million of displaced people are living in low-cost temporary accommodations, in which forcibly displaced people may end up living for years or even decades [21–25]. In this framework, it is imperative for cities and governments to develop and provide durable and low-cost housing solutions for the lower-income and poorest population and for displaced people, in order to curb the growth and creation of slums, to ensure a resilient and sustainable urban development and to respect the everyone's right to have an adequate standard of living [16].

Lightweight prefabricated construction systems are often proposed as an affordable housing solution, to solve the increasing global housing demand, and as temporary housing units in emergency scenarios [10,11,26,27]. Thanks to the simultaneous adoption of prefabrication and value engineering, in fact, these technologies allow reducing delivery time and costs by up to 50 and 30%, respectively [16]. In particular, the use of standardized and prefabricated units or elements allows not only a quick, inexpensive and on a larger scale delivering, but also the reduction of energy consumption and wastes during the construction stages [28,29] due to the improvement of worksite safety, productivity and quality [30–32]. The impact of the buildings at the end of their life is also minimized due to the possibility of disassembling and/or

relocating the prefabricated modules [33–35]. Value engineering, instead, allows meeting specific economic targets through the minimization of not strictly necessary costs. This is usually obtained by "de-specifying" building requirements, such as, for example, minimum ceiling heights, amount of electrical or plumbing fixtures, but also varying characteristics of building components, favoring the use of cheaper ones [16].

Due to this, it is not uncommon that durability issues may occur during the service life of these buildings, especially if an adequate investigation on the aging processes of these low-cost building components is not accurately carried out [36]. Studies on affordable or temporary lightweight construction systems, in fact, often neglect durability aspects, mainly focusing on energy performance and thermal comfort (see e.g. [22,34,36–43]). An adequate investigation on durability aspects of these new building components and construction systems is then strongly needed to ensure a specific building performance and to predict correctly their actual life span, but also to avoid undesirable maintenance and repairing costs during their service life and to assess efficiently their life cycle cost and environmental impact [15,35].

This paper presents the research results of an experimental campaign aimed at investigating the durability in outdoor environments of a novel EPS-based lightweight prefabricated construction system, named HOMEDONE, specifically developed for affordable housing and temporary accommodation. The HOMEDONE construction technology is based on the assembly of prefabricated structural reinforced-EPS panels internally reinforced with a 3D steel wire mesh and externally topped off with a thin and continuous multi-layer rendering system. This system can be used to obtain in a few days even multi-story buildings, and several buildings were just built to obtain low-cost districts in developing countries and temporary emergency camps in post-earthquake scenarios [44].

As evidenced by similar technologies that adopt thin multilayer rendering systems on EPS panels (for which, however, a satisfactory body of knowledge about their long-term properties and durability is still lacking [45,46]), the durability of the HOMEDONE system is strongly related to the durability of its external finishing layers [47–52]. In fact, due to the high thermal resistance of the EPS panels, the outermost rendering layer reaches very high temperatures in summer (even 70°C), which can suddenly drop when, for example, a rainstorm occurs [37,53,54]. These high-temperature variations, along with the water content variations, cause different deformations among layers that may cause cracks or detachments of the finishing layers from the background [3,5,6,50,55]. Clearly, since the studied system is composed of a set of panels whose external continuity is ensured only by the external finishing system, these cracks may turn in (or be a symptom of) a loss of performance of the entire system [45,48,49,55–57]. Then, it is important to investigate the possible occurrence of cracks and detachments on the external rendering systems.

With this aim, in this work, the thermal compatibility among the different layers of the HOMEDONE construction system is investigated with appropriate accelerated aging tests, i.e. freeze-thaw tests and wet/drying and UV tests. These tests involve the most relevant atmospheric agents affecting the durability of EPS walls with multilayer rendering systems, such as thermal shocks, UV radiation and variations in water contents (driving rain) [3,8,9,47,58], excepting for physical and chemical agents such as pollutants that have been not considered in this study [48]. During tests, the development of cracking, detachments and variations in bonding strength between different layers have been then measured. Attenuated Total Reflection Fourier-Transform Infrared (ATR-FT-IR) spectroscopic analyses have been carried out to understand the effects of aging processes on a micro-scale [59–61]. X-Ray Diffraction (XRD) and ATR-FT-IR analyses have been also carried out to characterize the different finishing materials. This experimental campaign represents the initial stage of a wider research program on the hygrothermal performance of HOMEDONE panels [62].

2 MATERIALS AND METHODS

2.1 Phases

This paper can be subdivided into two main phases.

In the first phase, a characterization of the different finishing materials applied on the EPS-reinforced panels is carried out through X-Ray Diffraction (XRD) and Attenuated Total Reflectance Fourier Transform Infrared Spectroscopy (ATR-FT-IR) analyses in order to evaluate their composition and to extend the findings to broader applications.

In the second phase, the effects of atmospheric agents (such as thermal shock, UV radiation, driving rain, etc. [48]) on the HOMEDONE panels have been evaluated by carrying out aging tests typically adopted in literature for similar technologies [3,8,9,47,58]. In particular, considering the absence of specific standards for reinforced-EPS construction systems, testing procedures commonly adopted for assessing the thermal compatibility between rendering systems and different substrates (as EPS [63–65] and concrete [66]) have been taken as reference, i.e.:

- Freeze-Thaw tests according to EN 13687-4:2003 [66];
- Wet/Drying and UV tests according to EN ISO 16474-3:2016 [67].

The effects of the two different aging cycles on the external layers of the samples have been monitored by using both non-destructive and destructive tests. Firstly, macroscopic variations of the external layers caused by aging have been assessed by spectrophotometric analyses (in the visible wavelength range) and visual inspections. Then, changes on the microstructure, which have an important meaning for macroscopic properties such as strength, water absorption, frost-proof, etc. [6], have been assessed by using ATR-FT-IR analyses [59–61]. Finally, since bond strength is a key factor for determining the thermal compatibility between layers of a wall covering [68], bond strengths have been also determined through pull-off tests after Freeze-Thaw tests, as prescribed in EN 13687-4:2003 [66].

2.2 HOMEDONE construction system

The HOMEDONE construction system is a lightweight relocatable prefabricated construction system based on the assembly of prefabricated reinforced-EPS panels. Specifically developed for affordable and temporary housing solutions, it takes advantage of industrial automated construction processes and value engineering to reduce housing delivery time and costs. In particular, it allows delivering both ready-made units (totally made off-site and then shipped on-site) and kit supplies (involving the shipping of prefabricated and modular elements for the on-site assembly). The latter are very useful for areas where, due to difficult access, heavy transport systems such as crane cannot be used [69].

Each reinforced-EPS panel (Fig. 1b) consists of a high strength tridimensional electro-welded galvanized steel wire (S235JR [70] steel bars with a diameter of 3 mm), embedded in a high-density EPS panel (from 45 kg/m^3 to 65 kg/m^3).

Depending on the structural and architectural needs, the panels and the embedded steel wires can be provided in different shapes and dimensions, allowing the construction of buildings of any size. The steel mesh is provided with metal joints, designed to easily connect roof and wall panels. Thanks to a patented hooking system, in fact, panels can be manually assembled on-site by using a simple Allen wrench (Fig. 1). This is very useful in emergency situations or, in general, in places where skilled workers are not present as in developing countries [71].

After the assembling, the external surfaces are topped off with a continuous thin multi-layer rendering system (with an overall thickness of 4 mm [68]). This latter includes three layers: a cement-based base coat reinforced with a glass fiber mesh (generally 5x5mm); a key coat, which acts as a preparation for the application of a finishing coat; a finishing coat, which contributes to the protection against weathering and provides a decorative finish (Fig. 1b). Due to its lightweight, the assembled building can be easily relocated and different units can be combined with each other to meet the needs of the inhabitants or to allow different use (i.e. temporary housing, affordable housing or for tourism).

In order to study the durability of the system, in this work, a single panel typically adopted for one-story constructions is taken as reference. This panel is characterized by a thickness equal to 10 cm and an EPS density of 45 kg/m^3. The dimensional characteristics of the tridimensional steel wire are reported in Fig. 2.

As previously said, the weakest part of this construction system is the external multi-layer rendering system, i.e. that directly exposed to the weathering action. In the external surface, in fact, very high temperature and water content variations can occur, due to the high thermal resistance of the structural EPS panels. For this reason, different finishing systems have been considered in this study, i.e. those directly provided by the HOMEDONE manufacturer for different climatic conditions, in order to identify the most suitable for use. In particular, these systems involve three different cement-based base coat mortars and five different types of white finishing coats.

Base coats are made of a ready dry mixture of cement binder and sand fillers smaller than 0.5, 0.7 and 1.2 mm for the basecoat 1, 2 and 3, respectively. The adopted finishing coats, instead, are characterized by different resin types, i.e. acrylic (A1 and A2), acrylic siloxane (AS and S) and styrene-acrylic (StA) resins. It is known, in fact, that different resin types may behave differently when subjected to aging cycles [5,47]. The main characteristics and the nomenclatures of the multi-layer rendering systems subject to the aging test are listed in Table 1. For the sake of brevity, the key coats are not reported since strictly related to the related finishing coat.

Before carrying out aging tests, qualitative and quantitative information on the thermal performance variation of the chosen panel, due to the presence of the embedded steel bars have been collected. In particular, first a qualitative estimation of the surface temperatures variation on the panel surface was obtained through an active infrared thermographic analysis on a panel purposely heated at 55°C [72–74]. At this aim, a *Mikron 7800 Infrared Camera* was used, while climatic data, emissivity value (set equal to 0.95 [75]) and the distance of the thermal camera from the target area were set up into the *NRG Pro software v.1.997* to obtain a good estimation of the temperatures. Then, in order to evaluate the thermal performance variation of a panel in real use conditions, surface temperatures and heat fluxes were measured in different points of a real panel used to build an experimental mock-up (see [62]). As a result, the IR camera showed a temperature difference on the panel surface of about 0.25°C when the IR photo was taken (Fig. 3). The *in situ* survey showed no significant variations between the measured surface temperatures and between heat fluxes, denoting a sufficiently good homogeneity of the panel in terms of thermal performance in real use conditions [62].

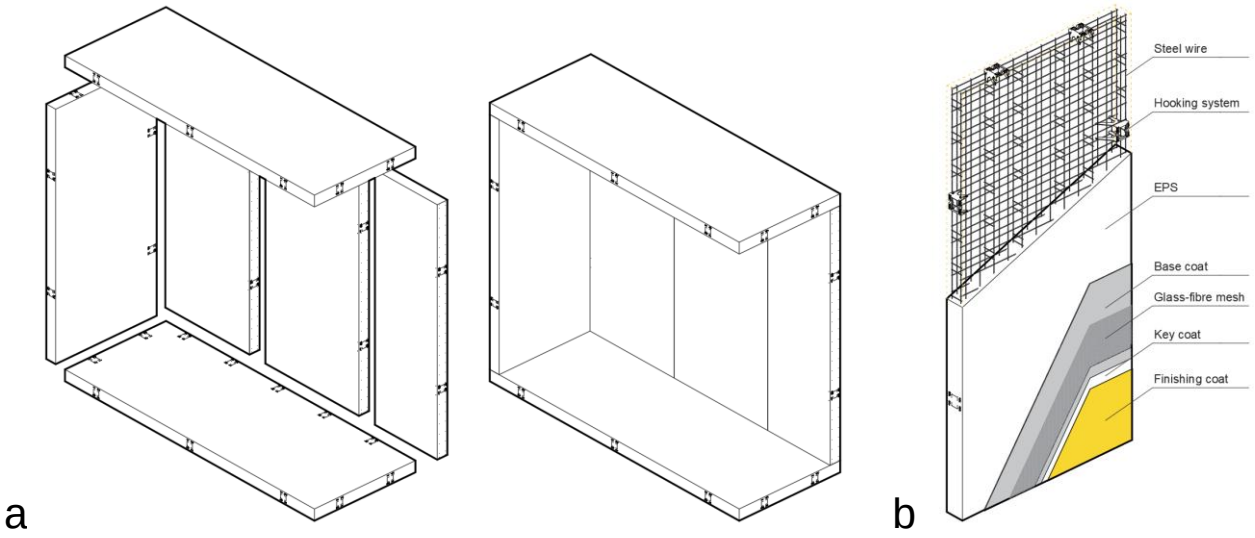

Fig. 1. a) Axonometric view of the assembly process of reinforced-EPS panels; b) axonometric view of reinforced-EPS panels adopted in this study with the description of the multi-coat rendering system.

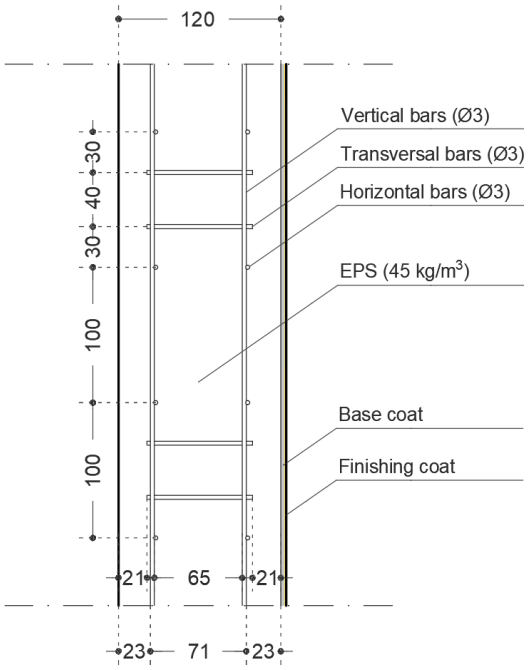

Fig. 2. Main geometrical data of the reinforced-EPS panels adopted in this study. Dimensions in millimeters.

Table 1. Identification and composition of the HOMEDONE multi-layer rendering systems with the most relevant properties according to the technical datasheets.

Rendering system ID	Base coat			Finishing coat				
	ID	Width (mm)	ETA	ID	Kind of resin	Width (mm)	ETA	Fibred
1-AS	1	3±0.2	06/0149	AS	Acrylic siloxane	1.2±0.2	08/0252	Yes
1-A1				A1	Acrylic	1.2±0.2	07/0200	Yes
1-A2				A2	Acrylic	1.5±0.2	-	No
1-StA				StA	Styrene acrylic	1.2±0.2	-	Yes
2-AS	2	3±0.2	-	AS	Acrylic siloxane	1.2±0.2	08/0252	Yes
2-A1				A1	Acrylic	1.2±0.2	07/0200	Yes
2-S				S	Acrylic siloxane	1.0±0.2	07/0200	No
2-StA				StA	Styrene acrylic	1.2±0.2	-	Yes
3-AS	3	3±0.2	04/0033	AS	Acrylic siloxane	1.2±0.2	08/0252	Yes
3-A1				A1	Acrylic	1.2±0.2	07/0200	Yes
3-S				S	Acrylic siloxane	1.0±0.2	07/0200	No
3-StA				StA	Styrene acrylic	1.2±0.2	-	Yes

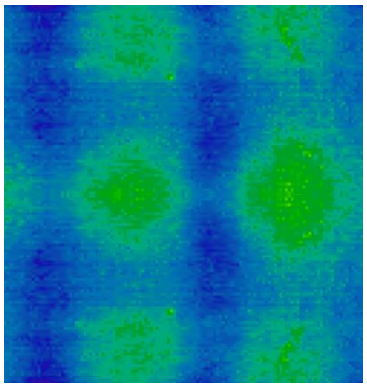

Fig. 3. Thermal IR image of the heated sample. Surface temperatures vary from about 23.75 °C (dark blue points) to about 24.00 °C (light green points).

2.3 Material characterization

2.3.1 X-ray diffraction (XRD) analyses

X-ray diffraction (XRD) is a powerful nondestructive technique for material characterization based on Bragg's law, able to provide information on structures, phases, preferred crystal orientations (texture), as well as average grain size, crystallinity, strain and crystal defects [3,5,76]. In particular, a monochromatic beam of X-rays is projected into the sample, and the reflected X-rays are then analyzed by a detector. A diffraction pattern is thus obtained, which can be considered as a fingerprint of the periodic atomic arrangements of the material under investigation, where broad peaks are produced by the amorphous regions of the samples while sharp peaks are produced by the crystalline regions.

In this study, XRD analyses have been carried out on powdered hydrated base coats samples in order to evaluate the microstructural composition of the adopted base coats materials before aging [3,5]. At this aim, an X-Ray diffractometer *RX Philips PW 1730*, with CuKa radiation, have been used, scanning at a diffraction interval of 5–70° with speed of 0.2°/min at 40kV voltage and 30 mA current intensity.

2.3.2 Attenuated Total Reflection Fourier Transform IR (ATR-FT-IR) spectroscopy

Attenuated Total Reflection Fourier Transform IR (ATR-FT-IR) spectroscopy is a sampling technique used in conjunction with infrared spectroscopy, in transmission or reflection modes, which enables samples to be examined directly in the solid or liquid state without further preparation [59].

An ATR accessory operates by measuring the changes occurring in a totally internally reflected infrared beam after interacting with the sample: the beam is directed onto an optically dense crystal with a high refractive index at a certain angle. This internal reflectance creates an evanescent wave that extends beyond the surface of the crystal into the sample in contact with it. In those regions of the IR spectrum in which the sample absorbs energy, the evanescent wave will be attenuated, returns back to the crystal, then exits in the opposite end towards the detector of the IR spectrometer which, in turn, records the attenuated beam as an interferogram, which is further transformed (FT) in an IR spectrum. For ATR measurements, the infrared beam protrudes only a few microns (0.5 μm - 5 μm) beyond the crystal surface and into the sample, hence the penetration depth of IR light is independent of the sample thickness.

In this study, ATR-FT-IR measurements have been carried out to acquire the spectra of the resins 1A2 (acrylic resin), 2A1 (acrylic resin), 2S (acrylic siloxane resin), 2StA (styrene-acrylic resin) and 2AS (acrylic siloxane resin) reported in

Table 1. Spectral analyses have been carried out both on the original resin samples, used as controls, and on those subjected to aging treatments through freeze-thaw cycles (FT) and UV-wetting cycles (UV), in order to determine the occurrence of microscopic variation after aging.

The samples have been analyzed by means of a *Perkin-Elmer Spectrum GX FT-IR System* spectrophotometer equipped with ATR single reflection diamond (*Senior Tecnologies DURA SamplIR II*) in the range between 4000 – 500 cm^{-1}, with a spectral resolution of 4 cm^{-1} and recording 32 scans. For this kind of measurement, the samples have been directly deposited on the measuring surface without requiring any preparation. In particular, a small amount of each resin has been placed on the ATR crystal and measurement has been carried out immediately. Identical experimental conditions have been maintained for all samples, and the background adsorption spectrum has been recorded each time for correction. *Spectrum 5.3.1* (*Perkin-Elmer*) has been used as the operating software.

2.4 Freeze-thaw test

For each applied rendering system (

Table 1), three 20x20x10 cm (B x H x W) samples have been prepared and cured for 7 days at the normalized temperature and relative humidity (RU) of the laboratory (21 ± 2 °C and 60 ± 10 %, respectively). One sample, marked as "*a_FT*"

sample, has been stored in the laboratory and used as a reference sample. The other two, marked as "*b_FT*" and "*c_FT*", have been subjected to 30 freeze-thaw cycles (Fig. 4) according to EN 13687-4:2003 [66] and EN 1504-3:2006 [77].

The effects of freeze-thaw cycles on the rendering systems have been assessed every 10 freeze-thaw cycles (i.e. at t_1, t_2 and t_3) in terms of surface defects (degree of blistering, cracking and flaking according to EN ISO 4628-1:2016 [78]) and chromatic alterations (according to ISO/CIE 11664-6:2014 [79]). The final assessment (t_3) has been carried out after 16h from the end of the last cycle [66].

In particular, digital images have been acquired through a 4800 x 9600 dpi resolution scanner (*HP G3010*) and a *Dino Lite Edge* digital microscope. In the latter case, nine 10x images of about 5x6.25 mm at nine fixed locations have been taken at each time interval.

Spectrophotometric analyses in the 340-740 nm wavelength range have been carried out by using a *Konika Minolta Cm.2600d* spectrophotometer. Colorimetric alterations have been assessed by following the CIELAB method according to ISO/CIE 11664-6:2014 [79]. The CIELAB method defines colors through three different coordinates of the CIELAB space measuring lightness (L^*), green to red (a^*) and blue to yellow (b^*) hue variations. For each specimen, and at each time interval, twenty-five measurements in terms of CIELab coordinates have been taken on twenty-five fixed locations in order to allow precise repeated measurements in the same points every time interval. Each measurement has been recorded as the mean of three. The color differences ΔE have been computed for each measuring point by comparing the measured coordinates before testing (t_0) with those measured at each time interval according to the procedure described in ISO/CIE 11664-6:2014 [79]. The differences in terms of lightness and chromaticity between two different colors, i.e. ΔL^*, Δa^* and Δb^*, have been also monitored.

Before and after aging, pull-off tests (EN 1542:1999 [80]) and ATR-FT-IR spectrophotometric analyses in the 2.5 – 20 µm (4000 – 500 cm^{-1}) wavelength range (described in section 2.5) have been also carried out. Pull-off tests are important for investigating the behavior of the wall covering material through its service life. In this study, a *CONTROLS Pull-Off/Bond strength digital tester 58-C0215* with accuracy equal to 1% has been used. In particular, according to the European Standard EN 1542:1999 [80], after a curing period of 7 days from the end of the test, five pull-off tests have been carried out on the fixed locations shown on both aged ("*b_FT*" and "*c_FT*") and not-aged ("*a_FT*") samples.

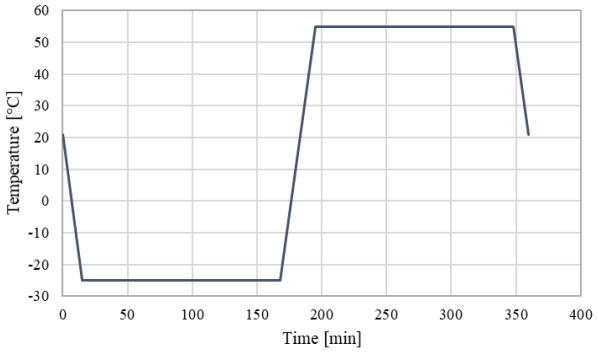

Fig. 4. Freeze-Thaw cycle adopted in this study.

2.5 Wet/drying and UV test

Wet/drying and UV tests have been carried out by taking as reference the testing procedure reported in EN ISO 16474-3:2016 [67]. In particular, for each rendering system, four 12.5x12.5x10 cm (B x H x W) samples have been prepared (Fig. 5) and cured for 7 days at the normalized temperature and RU of 23 ± 2 °C and 50 ± 5 %, respectively. According to EN 1062-11:2002 [81], three samples, marked as "*b_UV*", "*c_UV*" and "*d_UV*", have been subjected to 42 days of wet/drying and UV cycles. One sample, namely "*a_UV*", has been used as a reference sample and stored in a dark room at 23 ± 2 °C and 50 ± 5 % RU.

Each cycle of exposure has lasted 6 hours and consisted of 5 hours of UV exposure at 35 ± 3 °C and 1 hour of water spray at 25 ± 3 °C. The adopted UV lamp emits across the entire spectrum of the UV light, with peak emission in the UVA range at 366 nm. The water spray technique has been adopted for wetting the specimen due to the low conductivity of the samples [67].

The effects of thermal cycles on the external layer of the specimens have been assessed in terms of surface defects, chromatic alterations and possible changes in their FT-IR spectra. According to ISO 16474-1:2013 [82], the surfaces of the tested samples have not been washed or cleaned before the measurements. In particular, surface defects and chromatic alterations have been assessed before testing (t_0) and after every week (t_1, t_2, t_3, t_4, t_5 and t_6) by using the same instruments and methodologies described in section §0. Even in this case, the measurement points have been localized by a reference spatial grid to ensure precise repeated measurements in the same locations. Before color measurements, the specimens have been left to dry at the laboratory temperature for approximately 3h in order to minimize the color changes of the surfaces caused by the water content in the external layers. An additional color measurement has been also taken after a curing period of 24h in order to determine the color stability after exposure.

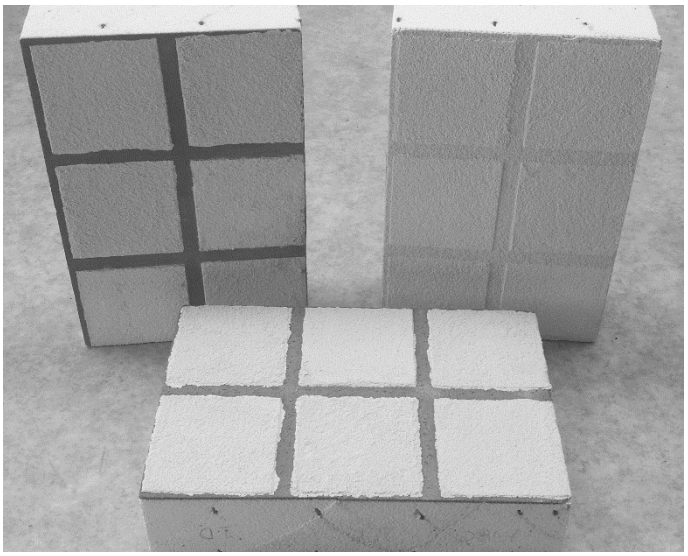

Fig. 5. Specimens prepared for the wet/drying and UV test.

3 RESULTS

3.1 Materials characterization

3.1.1 XRD analyses

Powdered samples of hydrated base coats have been investigated by means of XRD analyses spectroscopy, as described in section 2.3.1, in order to characterize the adopted base coats materials by evaluating their microstructural composition and then to extend the results to broader applications.

XRD results of the 1, 2 and 3 basecoats after 28-day of hydration are reported in Fig. 6. As expected, the diffraction bands show the presence of cement binder components like alite and calcite in all the analyzed materials, as observed for similar thin-layer plaster typically applied on EPS or cement substrates (see e.g. [5]). The basecoats mainly differ from each other due to the use of different types of sand filler. In particular, for basecoats 1 and 2, the most often detected peak is related to quartz that, along with mica, chlorite and natural silicates, indicates the use of natural silica sand filler for manufacturing the two mortars [5]. Differently, for basecoat 3, the presence of ankerite is observed, denoting the use of carbonate sand instead of silica sand [83].

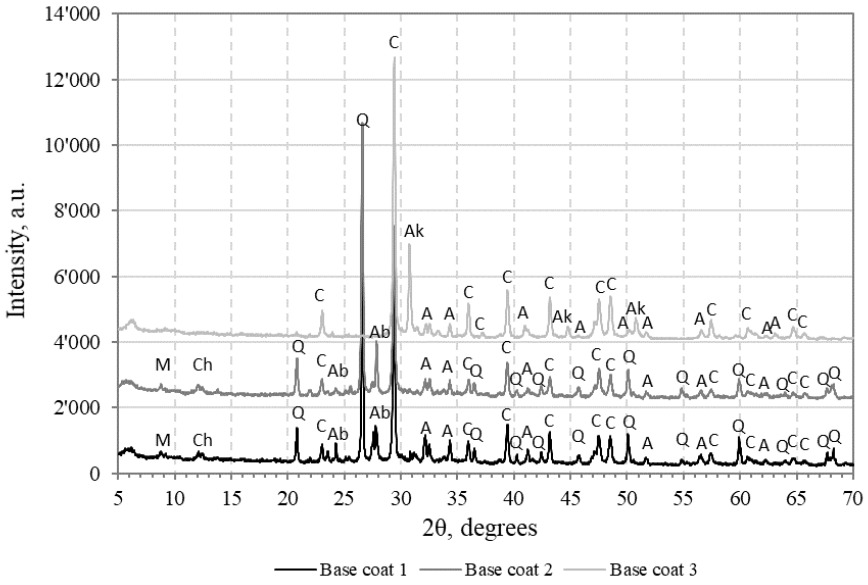

Fig. 6. XRD analysis of 1, 2 and 3 basecoats (A – Alite, C – Calcite, Q – Quartz, Ab – natural silicates (albite), M – Mica, Ch – Chlorite, Ak – Ankerite).

3.1.2 ATR-FT-IR analyses

Aliquots from the untreated samples have been investigated by means of ATR-FT-IR spectroscopy as described in section 2.3.2, in order to characterize the different samples. As a result, all resins analyzed have been found to be charged with large quantities of calcium carbonate as a filler, whose characteristic spectral bands (at 2872, 2513, 2140, 1795, 1739, 1377, 873 and 712 cm^{-1}) resulted superimposed with those corresponding to the organic matrix of each sample, hence hampering a proper characterization. In Fig. 13Fig. 7, the non-aged 2StA IR spectrum has been reported as a representative example.

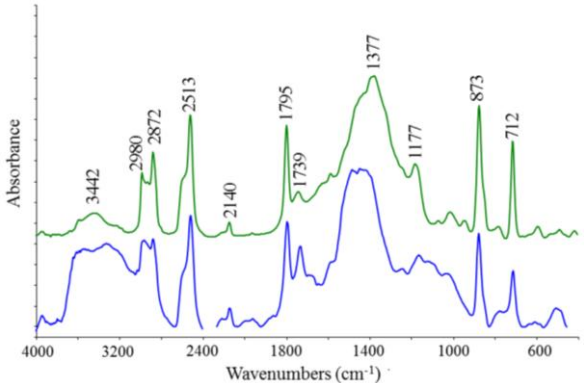

Fig. 7. IR spectra comparison of calcium carbonate alone (black), 2StA (blue), in the 4000-450 cm^{-1} region.

In order to perform a correct characterization, the organic matrix present in each sample has been separated from the calcium carbonate by overnight extraction with chloroform at room temperature. After solvent evaporation of these extracts at reduced pressure, the resulting organic residues have been analyzed in transmission mode, and the characteristic spectral bands of the polymers in the samples resulted clearly visible allowing their identification. This procedure has been successfully employed for all non-aged samples (1A2, 2A1, 2S, 2StA, 2AS), and some results have been reported in Fig. 8. In particular, the spectra of 2StA, 2S and 2A1 are shown in Fig. 8, as representative of the three different types of organic matrix found in the samples under investigation.

In particular, by comparing the spectrum of non-aged 2StA resin with those present in the database available from the instrument used (*Perkin-Elmer*), the correspondence with the spectrum of a styrene-acrylic resin was clearly evident, according to what reported in Table 1; similarly, the spectra of 2S and 2A1 resulted attributable to an acrylic siloxane and an acrylic resin respectively.

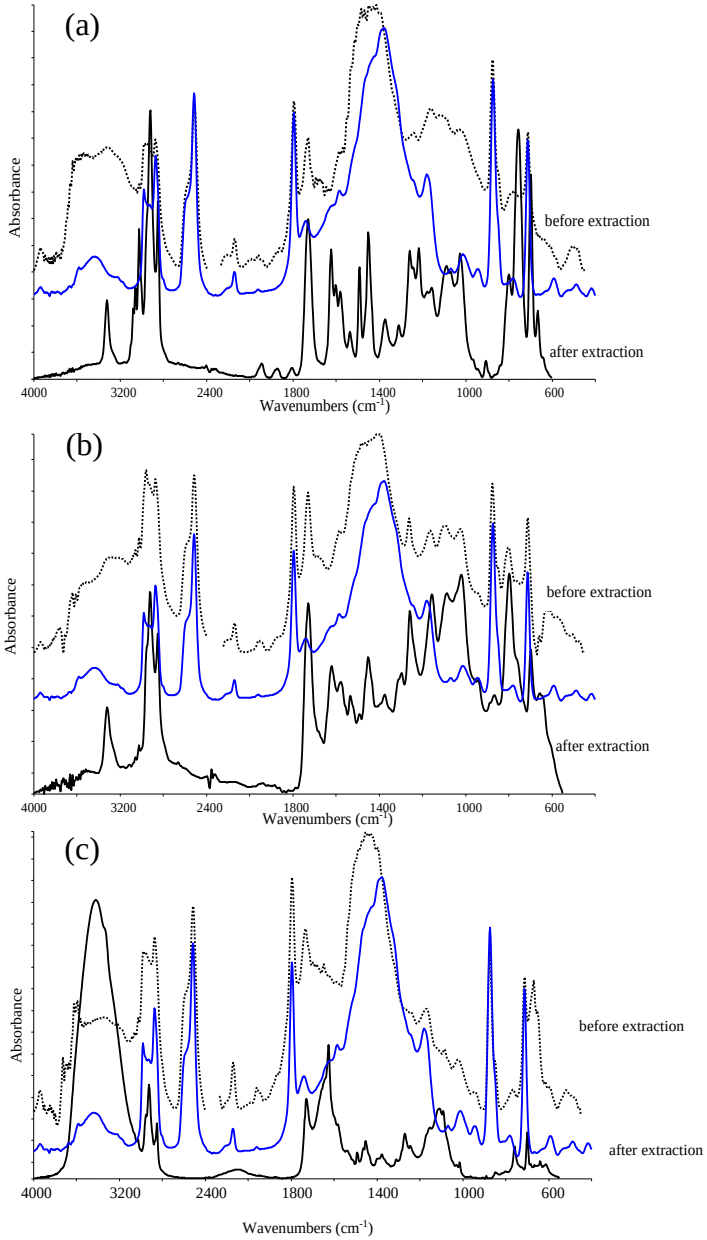

Fig. 8. Comparison between IR spectra of 2StA (a) 2S (b) and 2A1 (c) before (dotted black lines) and after (solid black lines) the extraction procedure in the 4000-450 cm^{-1} spectral region. The blue lines refer to the spectrum of pure calcium carbonate.

3.2 Freeze-thaw test

The results of visual inspections are summarized in Fig. 9, in which some representative digital image acquisitions are reported. As can be seen, the freeze-thaw cycles have not caused detachments or other visible alterations on the surface of the specimens.

The average color variations ΔE are reported in Table 2. In all cases, the obtained values are lower than the just noticeable difference (JND) fixed to 2.3 [84], which represents the physical threshold under which the human eye cannot perceive color differences. These values are also lower than 1, i.e. an alternative conventional threshold used in literature to identify slightly hue variations (see e.g. [85]), defined as the minimum threshold for 50% color match acceptability [86].

All the ΔE samples are characterized by high coefficients of variation (CoV). These range from 22% to 72% with a mean value equal to 44%, while the corresponding standard deviation values range between 0.11 and 0.30 with a mean value equal to 0.19.

Concerning pull-off tests, for both the aged and the non-aged samples, breaking has always occurred partially inside the base coat (cohesive breaking) and partially at the interface between the base coat and the insulation layer (adhesive breaking, see Fig. 10). From these results, it is clear that the interface between the base coat and insulation layer, as well as the base coat, represents the weakest points of the construction system.

Since the type of finishing coat has not affected the breaking mode, the tensile strengths obtained from the pull-off tests have been grouped by type of base coats and reported in form of box plot (Fig. 11). As it can be seen, each group of non-

aged specimen presents a median failure tension strength of about 0.09-0.10 MPa. This value is slightly higher than the minimum requirement set for similar technologies such as ETICS in reference documents (0.08 MPa [63,64]). Moreover, it should be noted that an increase in bonding strength is obtained due to aging. On average, this increase is about 6.1% for each base coat.

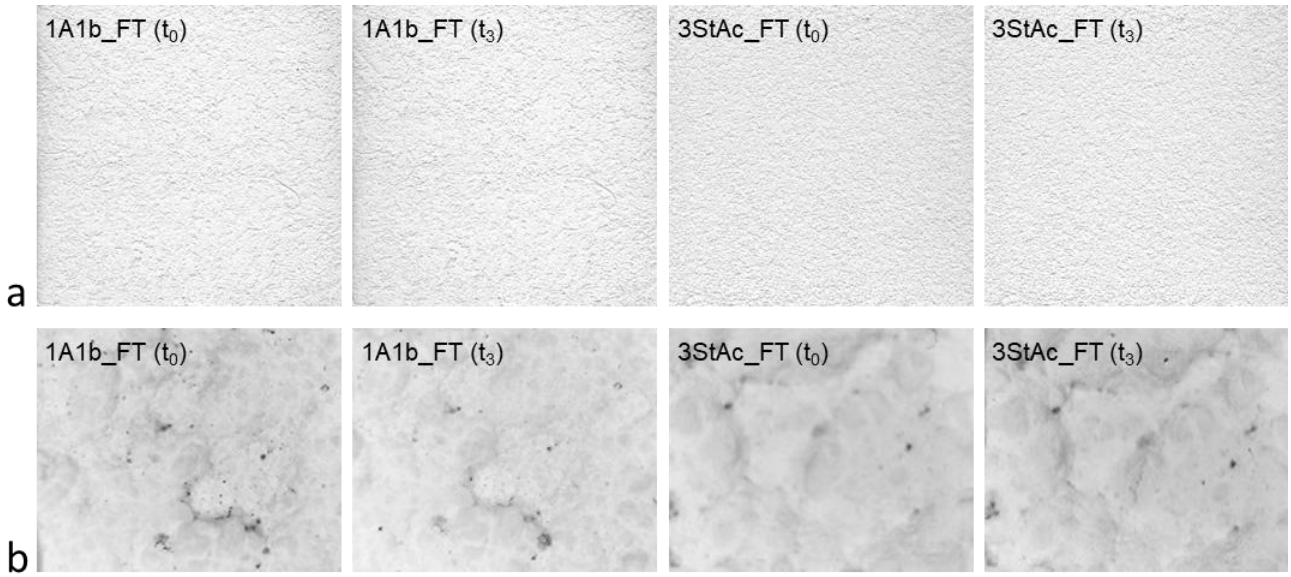

Fig. 9. Examples of digital images taken before (t_0) and after the freeze-thaw test (t_3) for the 1A1*b_FT* and 3StA*c_FT* specimens by using (a) digital scanner and (b) digital microscope.

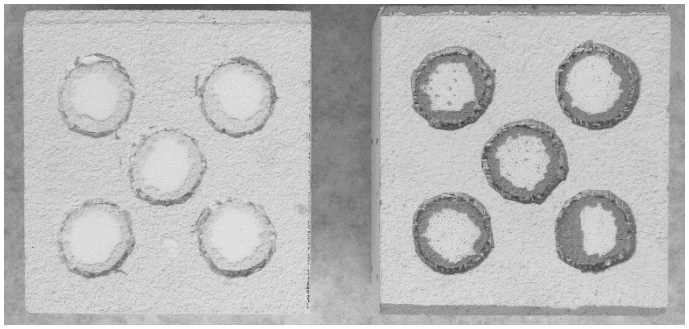

Fig. 10. Example of the failure mode in tensile bond strength tests.

Table 2. Mean color variations (ΔE) of the surface of the specimens calculated at each time interval due to freeze-thaw cycles.

Time interval	Rendering system ID											
	1-AS	*1-A1*	*1-A2*	*1-StA*	*2-AS*	*2-A1*	*2-S*	*2-StA*	*3-AS*	*3-A1*	*3-S*	*3-StA*
t_1	0.48	0.57	0.39	0.50	0.27	0.29	0.34	0.27	0.35	0.28	0.27	0.25
t_2	0.63	0.65	0.40	0.61	0.38	0.49	0.54	0.26	0.45	0.4	0.52	0.27
t_3	0.68	0.65	0.40	0.57	0.43	0.43	0.73	0.27	0.53	0.51	0.74	0.38

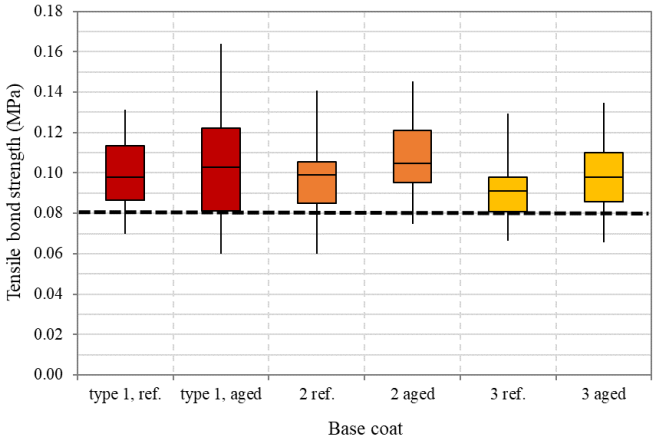

Fig. 11. Tensile bonding strength (MPa) of the rendering system before and after aging through freeze-thaw cycles. Results grouped by type of base coat.

3.3 Wet/drying and UV test

No detachments or other surface alterations due to the accelerated aging process have been observed after visual inspections. However, some slight color variations have been recorded in this case. For each multi-layer rendering system, Fig. 12 reports the average ΔE values computed at each time step. As can be seen, all the rendering systems have shown slight hue variations, i.e. ΔE values higher than 1 [85]. More in detail, according to the JND threshold (ΔE=2.30, [84]), specimens with StA and A2 finishing layers are the only ones that have maintained the original colors, while significant color variations (ΔE>2.30) have been obtained for specimens with the AS, A1 and S finishing coats. In

Table 3, the average color variations at the end of the test in terms of CIELab coordinates are reported. From these results, slight variations in L values, corresponding to less bright specimens (negative ΔL), and higher variations in b values, corresponding to less blue and more yellow specimens (positive Δb), can be observed. Concerning the scattering of the results, ΔE samples are characterized by a CoV ranging from 9% to 56% (average value equal to 21%), corresponding to standard deviations ranging from 0.19 to 0.72 (average value equal to 0.37).

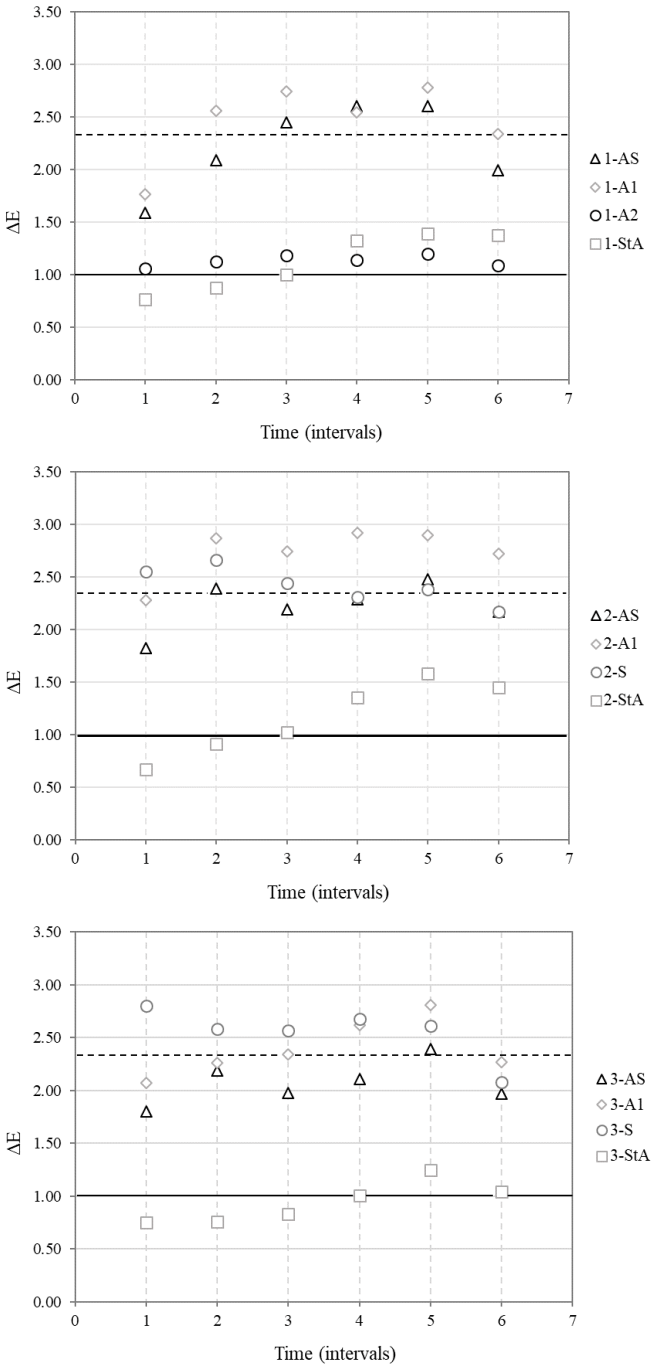

Fig. 12. Mean color variations (ΔE) at each time interval after wet/drying and UV cycles. The horizontal dashed line is the limit under which color differences are not visible to the naked eye (just notable difference JND, ΔE = 2.3 [84]). The horizontal solid line is a conventional threshold used in literature for slight hue variations (ΔE = 1, [85]).

Table 3. Average color variations at the end of the wet/drying and UV test expressed as CIELab color coordinates.

	Multi-layer rendering system ID											
	1-AS	*1-A1*	*1-A2*	*1-StA*	*2-AS*	*2-A1*	*2-S*	*2-StA*	*3-AS*	*3-A1*	*3-S*	*3-StA*
ΔL	-0.86	-0.88	0.20	-0.72	-0.79	-0.73	-0.55	-0.96	-0.84	-0.82	-0.68	-0.56
Δa	-0.09	-0.06	-0.09	-0.03	-0.03	0.02	-0.04	0.01	-0.05	-0.07	-0.08	-0.08
Δb	2.35	2.63	1.23	1.54	2.57	3.35	2.63	1.68	2.27	2.80	2.48	1.20

3.4 ATR-FT-IR analyses on aged samples

Aliquots from the aged samples from both treatments, i.e. freeze-thaw cycles (FT) and UV-wetting cycles (UV), have been investigated by means of ATR-FT-IR spectroscopy as described in section 2.3.2, in order to allow a comparison with the

corresponding non-aged samples. Overall, 15 different multi-layer finishing systems have been analyzed.

As already noted for non-aged samples, all the aged ones have been found to be charged with large quantities of calcium carbonate as a filler (see Fig. 13). For this reason, in order to separate the organic matrix from the calcium carbonate, the overnight extraction with chloroform at room temperature has been carried out even in this case (see Section 3.1.2).

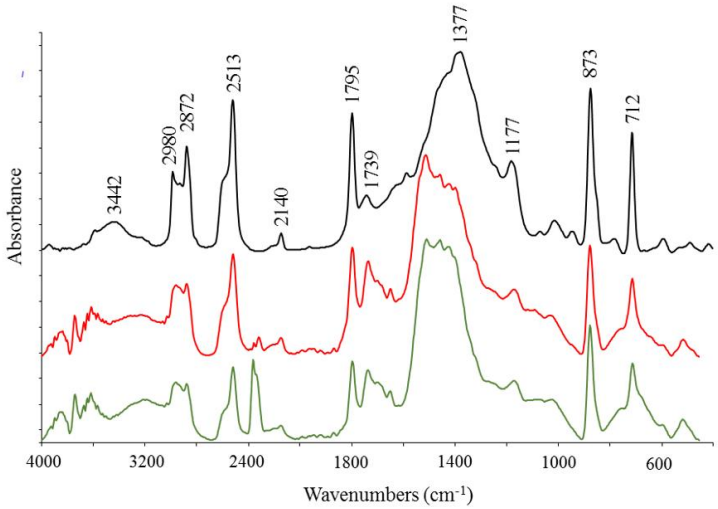

Fig. 13. IR spectra comparison of calcium carbonate alone (black), 2StA_*FT* (red), 2StA_*UV* (green), in the 4000-450 cm^{-1} region.

In Table 4, the results of the analysis carried out in transmission mode on the resulting organic residues from the solvent extraction procedure above described, are reported in terms of most relevant IR peak wavelengths, together with the corresponding vibrational assignments according to the literature, with the main spectral variations arising from both aging treatments in bold [87].

Peak wavenumber (cm^{-1})	Assignment
3322	**Overtone C=C**
3026	**ν =C-H**
2923	ν_{as} CH_2,CH_3
2851	ν_{s} CH_2,CH_3
1730	**ν C=O**
1624	**ν C=C**
1491	δ_{as} CH_2,CH
1451	δ_{s} CH_2,CH_3
1374	**ν COO-**
1260	δ $=CH_2$
1218	γ CH_2,CH_3
1155	γ CH_2,CH_3
1027	ν C-C
906	ν C=C
757	τ CH_2
699	ν C=C

Table 4. Wavenumbers (in cm^{-1}) of the most relevant IR bands in polymeric chains, together with the related vibrational mode marks. **ν**: stretching, **δ**: bending (s: symmetric, as: asymmetric), **γ**: twisting, **τ**: rocking. In bold the main spectral variations arising from both aging treatments.

Considering the organic residues from the solvent extraction procedure above described, the aging effects on the studied systems resulted more evident from the FT-IR study with respect to the findings of the chromatic tests. In particular, the spectral comparison of the organic matrix from the untreated and aged samples showed the typical changes arising from alkyl chains alterations due to incoming oxidative processes. These changes resulted always more evident in the UV-wetting cycles. In

Fig. 14, the spectral comparison of the styrene-acrylic resin 2StA with the corresponding aged ones, 2StA_FT and 2StA_DWUV, has been reported as a typical example.

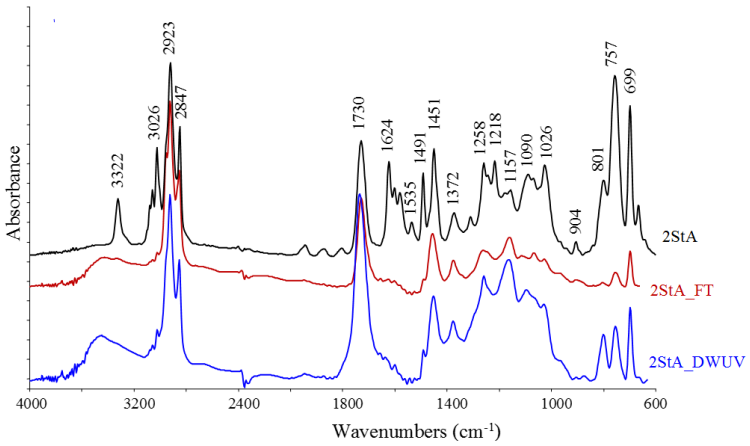

Fig. 14. Comparison between the chloroform extracts representative FT-IR spectrum of the non-aged resin 2StA (black) with those of the aged ones 2StA_FT (red) and 2StA_DWUV (blue).

The IR spectra there reported clearly show some differences arising from aging. In particular, the decreased intensity of the bands at 3026 and 1624 cm^{-1}, attributed to ν(=C-H) and ν(C=C) respectively, with instead an increase of the band at 1730 cm^{-1}, attributed to ν(C=O), because of incoming oxidative processes.

Similar behavior has been found for 2A1. In this case, the changes recorded after aging are more pronounced if compared with 2StA resin, as shown in Fig. 15. In fact, both bands at 3026 and 1624 cm^{-1}, attributed to ν(=C-H) and ν(C=C) respectively, dramatically decreased, together with the increase of the band at 1730 cm^{-1}, attributed to ν(C=O), recording even an inversion of the intensities between the 1624 and 1730 cm^{-1} bands.

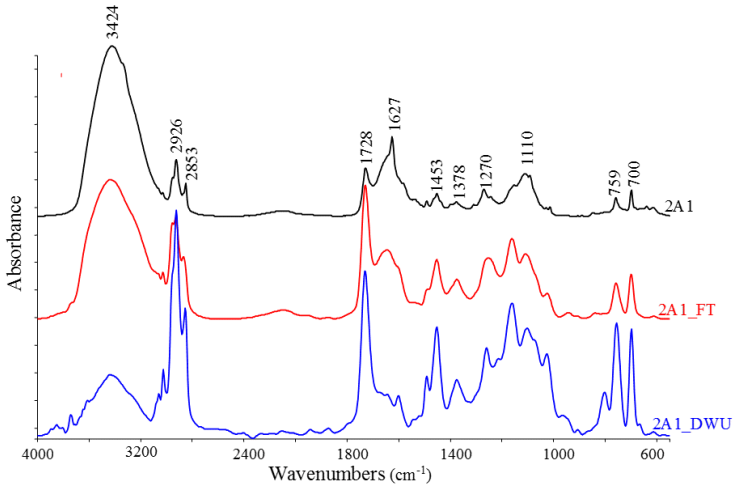

Fig. 15. Comparison between the chloroform extracts representative FT-IR spectrum of the non-aged resin 2A1 (black) with those of the aged ones 2A1_FT (red) and 2A1_DWUV (blue).

Finally, the differences between resin 2S and the corresponding aged ones 2S_FT and 2S_DWUV are shown in Fig. 16. In this case, the organic matrix is represented by an acrylic siloxane resin, hence a different behavior has been observed. However, due to the presence of hydrocarbon chains, changes relative to their aging are present, such as the decrease of bands intensities in the 3300 – 2800 cm^{-1} region (=C-H), also accompanied by the disappearance of the signal at 3322 cm^{-1} attributed to the corresponding overtone. In addition, significant changes occurred in the spectral pattern ranging between 1300 and 1000 cm^{-1}, suggesting that the aging processes deeply affects the resin backbone, where the incoming oxidation process promoted cross-linking and chain scission reactions [88].

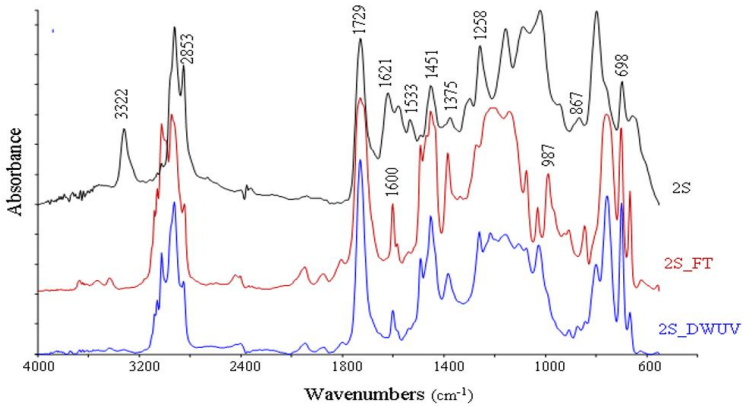

Fig. 16. Comparison between the chloroform extracts representative FT-IR spectrum of the non-aged resin 2S (black) with those of the aged ones 2S_FT (red) and 2S_DWUV (blue).

4 DISCUSSION

The tests carried out in this study have allowed investigating the durability of a reinforced-EPS based construction system in outdoor environments. After aging tests, which have involved the most important atmospheric agents affecting the durability of similar technologies (i.e. thermal shocks, UV radiations and temperature and water content variations), the finishing layers have not shown visible detachments, cracks or other visible defects on the different finishing coats. Then, the presence of the steel wire does not have affected the EPS deformability. This result is similar to that obtained for similar technologies (e.g. [47]), where no visible defects are present on finishing coating after UV cycles. In [47], this was attributed to the presence of TiO_2, able to reduce the transmittance of the UV radiations [89].

Concerning colorimetric analyses, only the wet/drying and UV aging test has caused visible color variations on all the samples. This has been probably due to the UV action that has affected the aesthetic appearance of the external layer, becoming less blue and more yellow [90]. In particular, positive Δb corresponding to a less blue and more yellow specimen, and negative ΔL values, corresponding to a less bright sample, have been obtained for all of the samples, with best results for specimens with StA (styrene-acrylic) and A2 (acrylic) finishing coats. This is similar to that obtained in [91], where a positive Δb and a negative ΔL of a white siloxane finishing coat applied on a reinforced concrete slate were obtained after four years of natural exposure in Milan, Italy. In particular, in [91] a stable value of Δb of approximately 3 was reached after aging. This value is comparable to that obtained in our work at the end of accelerated tests, ranging between 2.3 and 3.3 for the acrylic and acrylic siloxane resins. Conversely, ΔL values are less comparable. In fact, in [91] a ΔL value equal to -15 was obtained after the natural exposure in the urban environment, which is much higher than those obtained in our study (i.e. between -0.5 and -1). The obtained higher values can be attributable to the absence of pollution and dirt in the accelerated tests that, instead, are massively present in urban environments.

The tensile bond strength results indicate the good mechanical performance of the composite system before and after aging processes. In fact, the obtained tensile strengths values are higher than 0.8 MPa (i.e. the minimum requirement sets for ETICS in reference documents [63,64]). An increase of the tensile strength has been also registered after the aging process, probably due to the curing of the base coat during aging cycles. The breaking mode has not varied after the aging test. In particular, a mixed-mode has been obtained in all of the cases, with fracture lines developing inside the base coat between glass fiber mesh and the insulation layer, and at the interface between the base coat and insulation layer. This implies that the joints between the external multi-layer rendering system and reinforced-EPS panels, as well as the base coat, represents the weakest points of the construction system.

Finally, the FT-IR spectral variations observed after both aging treatments are diagnostic of autooxidative processes, which are more evident in UV cycles as expected in processes involving organic free radicals.

In fact, molecular oxygen plays an important role in aging and represents the main responsible of the olefin (C=C and C=C-H) moieties transformation in the organic polymeric fraction of the samples under investigation. In particular, these moieties are converted into the corresponding oxidation products characterized by the presence of carbonyl (C=O) moieties. In terms of IR spectra, this behavior produces the observed intensity decrease of the bands present in the region between 3300 – 2800 cm^{-1} as well as at 1624 cm^{-1}, typical of the C=C and C=C-H moieties, accompanied by an increased intensity of the C=O band at 1730 cm^{-1}, due to the formation of carbonyl derivatives, such as aldehydes, lactones and ketones, typical of hydrocarbon polymer chains oxidative degradation. In the styrene-acrylic resin 2StA, these changes occur to a minor extent, probably for a less reactivity due to the presence of the styrene moiety. On the other hand, siloxanes are known to be less reactive toward molecular oxygen, and the aging process behaves differently. In the acryl siloxane resin 2S, the hydrocarbon (acrylic) component follows the mechanism described above, while the siloxane one mainly undergoes cross-linking and chain scission reactions responsible of polymer backbone alterations, according to the significant changes observed in the spectral pattern in the IR region between 1300 and 1000 cm^{-1}.

However, all the specimens seem to resist satisfactorily to weathering actions.

5 CONCLUSIONS

In this study, the durability in the outdoor environment of a novel reinforced-EPS based construction system named HOMEDONE, developed for affordable and temporary housing solutions, has been investigated.

The results of this experimental campaign, which represents the initial stage of a wider research program on the hygrothermal performance of HOMEDONE panels, have pointed out the absence of significant defects on different external finishing layers after freeze-thaw cycles and wet/drying and UV cycles. After freeze-thaw cycles, pull-off tests results have shown good mechanical performance, even higher than the limits fixed by reference standards for ordinary ETICS with render finishing [63,64]. After wet/drying and UV cycles, some color variations have been recorded, with the best results obtained for specimens with styrene-acrylic and acrylic finishing coats. These results are comparable with those obtained for a siloxane finishing coat exposed for four years to the urban environment.

In addition, the present study indicates FT-IR spectroscopy as a powerful tool to investigate the incoming of degradation processes, even occurring to a small extent, due to its sensitivity with respect to chromatic tests, also allowing to evaluate the aging processes at a molecular level. Even in this case, the styrene-acrylic resin showed minor changes than other resins, probably due to the less reactivity caused by the presence of the styrene moiety.

In conclusion, the results obtained in this study indicate the HOMEDONE construction system as a promising and durable solution for affordable housing and emergency shelter. The thermal and hygrothermal behavior of such a system will be investigated in a further stage of the research.

6 ACKNOWLEDGMENTS

Financial support for this study was provided by the AC-Engineering S.p.A under the "POR FESR Marche 2014/2020" Research Project No. 15345.

7 REFERENCES

[1] P. Berdahl, H. Akbari, R. Levinson, W.A. Miller, Weathering of roofing materials-An overview, (2006). doi:10.1016/j.conbuildmat.2006.10.015.

[2] C.Y. Yiu, D.C.W. Ho, S.M. Lo, Weathering effects on external wall tiling systems, Constr. Build. Mater. 21 (2007) 594–600. doi:10.1016/j.conbuildmat.2005.11.002.

[3] J. Bochen, Weathering effects on physical–chemical properties of external plaster mortars exposed to different environments, Constr. Build. Mater. 79 (2015) 192–206. doi:10.1016/j.conbuildmat.2014.12.079.

[4] J. Souza, A. Silva, J. de Brito, E. Bauer, Service life prediction of ceramic tiling systems in Brasília-Brazil using the factor method, Constr. Build. Mater. 192 (2018) 38–49. doi:10.1016/j.conbuildmat.2018.10.084.

[5] J. Bochen, Study on the microstructure of thin-layer facade plasters of thermal insulating system during artificial weathering, Constr. Build. Mater. 23 (2009) 2559–2566. doi:10.1016/j.conbuildmat.2009.02.028.

[6] J. Bochen, S. Gil, Properties of pore structure of thin-layer external plasters under ageing in simulated environment, Constr. Build. Mater. 23 (2009) 2958–2963. doi:10.1016/j.conbuildmat.2009.02.041.

[7] N.L. Alchapar, E.N. Correa, Aging of roof coatings. Solar reflectance stability according to their morphological characteristics, Constr. Build. Mater. 102 (2016) 297–305. doi:10.1016/j.conbuildmat.2015.11.005.

[8] E. Franzoni, B. Pigino, G. Graziani, C. Lucchese, A. Fregni, A new prefabricated external thermal insulation composite board with ceramic finishing for buildings retrofitting, Mater. Struct. 49 (2016) 1527–1542. doi:10.1617/s11527-015-0593-7.

[9] A. Vilhena, C. Silva, P. Fonseca, S. Couto, Exterior walls covering system to improve thermal performance and increase service life of walls in rehabilitation interventions, Constr. Build. Mater. 142 (2017) 354–362. doi:10.1016/j.conbuildmat.2017.03.033.

[10] X. Gan, J. Zuo, P. Wu, J. Wang, R. Chang, T. Wen, How affordable housing becomes more sustainable? A stakeholder study, J. Clean. Prod. 162 (2017) 427–437. doi:10.1016/j.jclepro.2017.06.048.

[11] H. Wallbaum, Y. Ostermeyer, C. Salzer, E. Zea Escamilla, Indicator based sustainability assessment tool for affordable housing construction technologies, Ecol. Indic. 18 (2012) 353–364. doi:10.1016/j.ecolind.2011.12.005.

[12] Eurostat, Migration and migrant population statistics - Statistics Explained, (2018). http://ec.europa.eu/eurostat/statistics-explained/index.php/Migration_and_migrant_population_statistics (accessed December 27, 2017).

[13] Centre for Research on the Epidemiology of Disasters (CRED), The international disasters database, (2017). http://www.emdat.be/ (accessed December 27, 2017).

[14] S.M. Amin Hosseini, A. De La Fuente, O. Pons, Multi-criteria decision-making method for assessing the sustainability of post-disaster temporary housing units technologies: A case study in Bam, 2003, Sustain. Cities Soc. 20 (2016) 38–51. doi:10.1016/j.scs.2015.09.012.

[15] A. Atmaca, N. Atmaca, Comparative life cycle energy and cost analysis of post-disaster temporary housings, Appl. Energy. 171 (2016) 429–443. doi:10.1016/j.apenergy.2016.03.058.

[16] J. Woetzel, S. Ram, J. Mischke, N. Garemo, S. Sankhe, A blueprint for addressing the global affordable housing challenge, McKinsey&Company, 2014.

[17] UN-Habitat, United Nations Human Settlements Programme, (n.d.). https://unhabitat.org/ (accessed December

21, 2017).
[18] J. Woetzel, S. Ram, S. Peloquin, M. Limam, J. Mischke, Housing affordability: A supply-side tool kit for cities, McKinsey&Company, 2017.
[19] S.J. Kolo, F.P. Rahimian, J.S. Goulding, Offsite manufacturing construction: A big opportunity for housing delivery in Nigeria, Procedia Eng. 85 (2014) 319–327. doi:10.1016/j.proeng.2014.10.557.
[20] J. Woetzel, J. Mischke, S. Peloquin, D. Weisfield, A tool kit to close california's housing gap: 3.5 million homes by 2025, McKinsey&Company, 2016.
[21] UNRWA - United Nations Relief and Works Agency for Palestine refugees in the near east, Palestine refugees | UNRWA, (n.d.). https://www.unrwa.org/palestine-refugees (accessed September 19, 2018).
[22] R. Thapa, H.B. Rijal, M. Shukuya, Field study on acceptable indoor temperature in temporary shelters built in Nepal after massive earthquake 2015, Build. Environ. 135 (2018) 330–343. doi:10.1016/j.buildenv.2018.03.001.
[23] UNHCR - The UN Refugee Agency, UNHCR - Figures at a Glance. Statistical yearbooks, (2019). http://www.unhcr.org/uk/figures-at-a-glance.html (accessed September 19, 2018).
[24] IDMC, Global Internal Displacement Database | IDMC, (2019). http://www.internal-displacement.org/database (accessed September 19, 2019).
[25] IDMC, GRID 2018 | Global Report on Internal Displacement 2018, (2018). http://internal-displacement.org/global-report/grid2018/ (accessed September 19, 2019).
[26] F. Barbosa, J. Woetzel, J. Mischke, M.J. Ribeirinho, M. Sridhar, M. Parsons, N. Bertram, S. Brown, Reinventing Construction: A Route To Higher Productivity, McKinsey&Company, 2017.
[27] H.M. Bernstein, E.J. Gudjel, D. Laquidara-Carr, Prefabrication and Modularization: Increasing Productivity in the Construction Industry, McGraw-Hill Construction, 2011.
[28] N. Lu, The current use of offsite construction techniques in the united states construction industry, in: 2009 Constr. Res. Congr., 2009. doi:10.1061/41020(339)96.
[29] R.M. Lawson, R.G. Ogden, Sustainability and Process Benefits of Modular Construction, 8th CIB World Build. Congr. (2010).
[30] E.M. Generalova, V.P. Generalov, A.A. Kuznetsova, Modular Buildings in Modern Construction, in: Procedia Eng., 2016. doi:10.1016/j.proeng.2016.08.098.
[31] D. Lopez, T.M. Froese, Analysis of Costs and Benefits of Panelized and Modular Prefabricated Homes, Procedia Eng. 145 (2016) 1291–1297. doi:10.1016/j.proeng.2016.04.166.
[32] R.M. Lawson, R.G. Ogden, R. Bergin, Application of Modular Construction in High-Rise Buildings, J. Archit. Eng. (2012). doi:10.1061/(ASCE)AE.1943-5568.0000057.
[33] X.X. Li, G.L. Li, Exploration of Modular Build of Architectural Space, Appl. Mech. Mater. (2013). doi:10.4028/www.scientific.net/AMM.357-360.338.
[34] G. Tumminia, F. Guarino, S. Longo, M. Ferraro, M. Cellura, V. Antonucci, Life cycle energy performances and environmental impacts of a prefabricated building module, Renew. Sustain. Energy Rev. 92 (2018) 272–283. doi:10.1016/j.rser.2018.04.059.
[35] L. Aye, T. Ngo, R.H. Crawford, R. Gammampila, P. Mendis, Life cycle greenhouse gas emissions and energy analysis of prefabricated reusable building modules, Energy Build. 47 (2012) 159–168. doi:10.1016/j.enbuild.2011.11.049.
[36] D. Albadra, D. Coley, J. Hart, Toward healthy housing for the displaced, J. Archit. 23 (2018) 115–136. doi:10.1080/13602365.2018.1424227.
[37] Y. Wang, L. Wang, E. Long, S. Deng, An experimental study on the indoor thermal environment in prefabricated houses in the subtropics, Energy Build. 127 (2016) 529–539. doi:10.1016/j.enbuild.2016.05.061.
[38] L. Huang, E. Long, J. Ouyang, Measurement of the Thermal Environment in Temporary Settlements with High Building Density after 2008 Wenchuan Earthquake in China, Procedia Eng. 121 (2015) 95–100. doi:10.1016/j.proeng.2015.08.1027.
[39] M. Košir, N. Iglič, R. Kunič, Optimisation of heating, cooling and lighting energy performance of modular buildings in respect to location's climatic specifics, Renew. Energy. 129 (2018) 527–539. doi:10.1016/j.renene.2018.06.026.
[40] P. Samani, V. Leal, A. Mendes, N. Correia, Comparison of passive cooling techniques in improving thermal comfort of occupants of a pre-fabricated building, Energy Build. 120 (2016) 30–44. doi:10.1016/j.enbuild.2016.03.055.
[41] F. Barreca, V. Tirella, A self-built shelter in wood and agglomerated cork panels for temporary use in Mediterranean climate areas, Energy Build. 142 (2017) 1–7. doi:10.1016/j.enbuild.2017.03.003.
[42] D. Rockwood, J.T. da Silva, S. Olsen, I. Robertson, T. Tran, Design and prototyping of a FRCC modular and climate responsive affordable housing system for underserved people in the pacific island nations, J. Build. Eng. 4 (2015) 268–282. doi:10.1016/j.jobe.2015.09.013.
[43] P. Cherian, S. Paul, S.R.G. Krishna, D. Menon, A. Meher Prasad, Mass Housing Using GFRG Panels: A Sustainable, Rapid and Affordable Solution, J. Inst. Eng. Ser. A. 98 (2017) 95–100. doi:10.1007/s40030-017-0200-8.
[44] A.S. Sferra, Emergency: innovative prefabricated construction components for an eco-solidarity architecture, TECHNE - J. Technol. Archit. Environ. (2017) 328–334. doi:10.13128/Techne-20788.
[45] S. Ximenes, J. de Brito, P.L. Gaspar, A. Silva, Modelling the degradation and service life of ETICS in external walls,

Mater. Struct. 48 (2015) 2235–2249. doi:10.1617/s11527-014-0305-8.
[46] R. NORVAIŠIENĖ, G. GRICIUTĖ, R. BLIŪDŽIUS, J. RAMANAUSKAS, The Changes of Moisture Absorption Properties during the Service Life of External Thermal Insulation Composite System, Mater. Sci. 19 (2013) 103–107. doi:10.5755/j01.ms.19.1.3834.
[47] G. Griciutė, R. Bliūdžius, Study on the microstructure and water absorption rate changes of exterior thin-layer polymer renders during natural and artificial ageing, Medziagotyra. 21 (2015) 149–154. doi:10.5755/j01.ms.21.1.4869.
[48] B. Daniotti, R. Paolini, F. Re Cecconi, Effects of Ageing and Moisture on Thermal Performance of ETICS Cladding, in: V.P. de de Freitas, J.M.P.Q. Delgado (Eds.), Springer Berlin Heidelberg, Berlin, Heidelberg, 2013: pp. 127–171. doi:10.1007/978-3-642-37475-3_6.
[49] B. Daniotti, F.R. Cecconi, R. Paolini, R. Galliano, J. Ferrer, L. Battaglia, Durability evaluation of ETICS: analysis of failures case studies and heat and moisture transfer simulations to assess the frequency of critical events, in: 4th Port. Conf. Mortars ETICS, 2012.
[50] J. Šadauskienė, V. Stankevičius, R. Bliūdžius, A. Gailius, The impact of the exterior painted thin-layer render's water vapour and liquid water permeability on the moisture state of the wall insulating system, Constr. Build. Mater. 23 (2009) 2788–2794. doi:10.1016/J.CONBUILDMAT.2009.03.010.
[51] T. Kvande, N. Bakken, E. Bergheim, J.V. Thue, T. Kvande, N. Bakken, E. Bergheim, J.V. Thue, Durability of ETICS with Rendering in Norway—Experimental and Field Investigations, Buildings. 8 (2018) 93. doi:10.3390/buildings8070093.
[52] S.S. de Freitas, V.P. de Freitas, Cracks on ETICS along thermal insulation joints: case study and a pathology catalogue, Struct. Surv. 34 (2016) 57–72. doi:10.1108/SS-09-2015-0043.
[53] H. Shen, H. Tan, A. Tzempelikos, The effect of reflective coatings on building surface temperatures, indoor environment and energy consumption - An experimental study, Energy Build. 43 (2011) 573–580. doi:10.1016/j.enbuild.2010.10.024.
[54] E. Barreira, V.P. De Freitas, Experimental study of the hygrothermal behaviour of External Thermal Insulation Composite Systems (ETICS), Build. Environ. 63 (2013) 31–39. doi:10.1016/j.buildenv.2013.02.001.
[55] H. Xiong, J. Xu, Y. Liu, S. Wang, Experimental Study on Hygrothermal Deformation of External Thermal Insulation Cladding Systems with Glazed Hollow Bead, Adv. Mater. Sci. Eng. 2016 (2016) 1–14. doi:10.1155/2016/3025213.
[56] B. Amaro, D. Saraiva, J. De Brito, I. Flores-Colen, Inspection and diagnosis system of ETICS on walls, Constr. Build. Mater. 47 (2013) 1257–1267. doi:10.1016/j.conbuildmat.2013.06.024.
[57] J.A.R. Mendes Silva, J. Falorca, A model plan for buildings maintenance with application in the performance analysis of a composite facade cover, Constr. Build. Mater. 23 (2009) 3248–3257. doi:10.1016/j.conbuildmat.2009.05.008.
[58] S.H. Ding, D.Z. Liu, Durability evaluation of building sealants by accelerated weathering and thermal analysis, Constr. Build. Mater. 20 (2006) 878–881. doi:10.1016/j.conbuildmat.2005.06.026.
[59] M. Lopes, V. Mouillet, L. Bernucci, T. Gabet, The potential of Attenuated Total Reflection imaging in the mid-infrared for the study of recycled asphalt mixtures, Constr. Build. Mater. 124 (2016) 1120–1131. doi:10.1016/j.conbuildmat.2016.08.108.
[60] L.D. Poulikakos, S. dos Santos, M. Bueno, S. Kuentzel, M. Hugener, M.N. Partl, Influence of short and long term aging on chemical, microstructural and macro-mechanical properties of recycled asphalt mixtures, Constr. Build. Mater. 51 (2014) 414–423. doi:10.1016/j.conbuildmat.2013.11.004.
[61] F. Iucolano, D. Caputo, F. Leboffe, B. Liguori, Mechanical behavior of plaster reinforced with abaca fibers, Constr. Build. Mater. 99 (2015) 184–191. doi:10.1016/j.conbuildmat.2015.09.020.
[62] M. D'Orazio, G. Maracchini, An experimental investigation on the indoor hygrothermal environment of a reinforced-EPS based temporary housing solution, Energy Build. 204 (2019) 109500. doi:10.1016/j.enbuild.2019.109500.
[63] European Organisation for Technical Approvals (EOTA), ETAG 004 - Guidelines for European Technical Approval of External Thermal Insulation Composite Systems (ETICS) With Rendering, 2013.
[64] CEN, EN 13499:2005, Thermal insulation products fo building - external thermal insulation composite systems (ETICS) based on expanded polystyrene - specification, 2005.
[65] ASTM, ASTM E 2110-11 Standard terminology for exterior insulation and finish systems (EIFS), 2011.
[66] EN 13687-4 Products and systems for the protection and repair of concrete structures - Test method - Determination of thermal compatibility - Dry thermal cycling, (2002).
[67] ISO 16474-3:2013. Paints and varnishes - Methods of exposure to laboratory light sources Fluorescent UV lamps, (2013).
[68] T. Uygunoğlu, S. Özgüven, M. Çalış, Effect of plaster thickness on performance of external thermal insulation cladding systems (ETICS) in buildings, Constr. Build. Mater. 122 (2016) 496–504. doi:10.1016/j.conbuildmat.2016.06.128.
[69] D. Félix, D. Monteiro, J.M. Branco, R. Bologna, A. Feio, The role of temporary accommodation buildings for post-disaster housing reconstruction, J. Hous. Built Environ. 30 (2014) 683–699. doi:10.1007/s10901-014-9431-4.
[70] (CEN) European Committee for Standardisation, EN 10027-1: 2005 Designation systems for steels - Part 1: Steel

names, Eur. Stand. 3 (2005) 1–25.
[71] D. Félix, J.M. Branco, A. Feio, Temporary housing after disasters: A state of the art survey, Habitat Int. 40 (2013) 136–141. doi:10.1016/j.habitatint.2013.03.006.
[72] F. Barreca, C.R. Fichera, Thermal insulation performance assessment of agglomerated cork boards, Wood Fiber Sci. 48 (2016) 96–103.
[73] F. Barreca, G. Modica, S. Di Fazio, V. Tirella, R. Tripodi, C.R. Fichera, Improving building energy modelling by applying advanced 3D surveying techniques on agri-food facilities, J. Agric. Eng. 48 (2017) 203–208. doi:10.4081/jae.2017.677.
[74] E. Lucchi, Applications of the infrared thermography in the energy audit of buildings: A review, Renew. Sustain. Energy Rev. (2018). doi:10.1016/j.rser.2017.10.031.
[75] A.M. Tanyer, A. Tavukcuoglu, M. Bekboliev, Assessing the airtightness performance of container houses in relation to its effect on energy efficiency, Build. Environ. 134 (2018) 59–73. doi:10.1016/j.buildenv.2018.02.026.
[76] Y. Govaerts, R. Hayen, M. de Bouw, A. Verdonck, W. Meulebroeck, S. Mertens, Y. Grégoire, Performance of a lime-based insulating render for heritage buildings, Constr. Build. Mater. (2018). doi:10.1016/j.conbuildmat.2017.10.115.
[77] EN 1504-3:2006. Products and systems for the protection and repair of concrete structures. Definitions, requirements, quality control and evaluation of conformity. Part 3: Structural and non-structural repair, (2006).
[78] EN ISO 4628-1:2016. Paint and varnishes - Evaluation of degradation of coatings - Designation of quantity and size of defects, and of intensity of uniform changes in appearance - Part 1: General introduction and designation system, (2016).
[79] ISO/CIE 11664-6:2014. Colorimetry - Part 6: CIEDE 2000 Colour difference formula, (2014).
[80] EN 1542:1999. Products and systems for the protection and repair of concrete structures - Test methods - Measurement of bond strength by pull-off, (1999).
[81] EN 1062-11:2002. Paints and varnishes - Coating materials and coating systems for exterior masonry and concrete - Part 11: Methods of conditioning before testing, (2002).
[82] ISO 16474-1:2013. Paints and varnishes -- Methods of exposure to laboratory light sources General guidance, (2013).
[83] J. Lanas, J.L. Pérez Bernal, M.A. Bello, J.I. Alvarez, Mechanical properties of masonry repair dolomitic lime-based mortars, Cem. Concr. Res. (2006). doi:10.1016/j.cemconres.2005.10.004.
[84] G. Sharma, Digital color imaging handbook, CRC Press, 2003.
[85] E. Quagliarini, F. Bondioli, G.B. Goffredo, A. Licciulli, P. Munafò, Smart surfaces for architectural heritage: Preliminary results about the application of TiO2-based coatings on travertine, J. Cult. Herit. 13 (2012) 204–209. doi:10.1016/j.culher.2011.10.002.
[86] R.G. Kuehni, R.T. Marcus, An Experiment in Visual Scaling of Small Color Differences, Color Res. Appl. (1979). doi:10.1111/j.1520-6378.1979.tb00094.x.
[87] T. Gocen, S.H. Bayari, M.H. Guven, Conformational and vibrational studies of arachidonic acid, light and temperature effects on ATR-FTIR spectra, Spectrochim. Acta - Part A Mol. Biomol. Spectrosc. (2018). doi:10.1016/j.saa.2018.05.100.
[88] N.S. Tomer, F. Delor-Jestin, L. Frezet, J. Lacoste, Oxidation, Chain Scission and Cross-Linking Studies of Polysiloxanes upon Ageings, Open J. Org. Polym. Mater. 02 (2012) 13–22. doi:10.4236/ojopm.2012.22003.
[89] H. Fjellstrom, H. Hoglund, S. Forsberg, M. Paulsson, The UV-screening properties of coating layers: The influence of pigments, binders and additives, Nord. Pulp Pap. Res. J. 24 (2009) 206–212. doi:10.3183/NPPRJ-2009-24-02-p206-212.
[90] S. Cabral-Fonseca, J.R. Correia, M.P. Rodrigues, F.A. Branco, Artificial accelerated ageing of GFRP pultruded profiles made of polyester and vinylester resins: Characterisation of physical-chemical and mechanical damage, Strain. 48 (2012) 162–173. doi:10.1111/j.1475-1305.2011.00810.x.
[91] R. Paolini, A. Zani, T. Poli, F. Antretter, M. Zinzi, Natural aging of cool walls: Impact on solar reflectance, sensitivity to thermal shocks and building energy needs, Energy Build. 153 (2017) 287–296. doi:10.1016/j.enbuild.2017.08.017.